END
DATE
FILMED
04-82
DTIC

1.0

1.1

1.25 1.4 1.6

2.5

2.2

2.0

1.8

Application of Time-Resolved Spectroscopies
to the Study of
Energetic Materials — 1981

A Summary Report

J. M. SCHNUR

Optical Probes Branch
Optical Sciences Division

March 5, 1982

DTIC
ELECTE
MAR 2 6 1982

B

NAVAL RESEARCH LABORATORY
Washington, D.C.

82 03 26 056

DTIC FILE COPY

REPORT DOCUMENTATION PAGE

READ INSTRUCTIONS
BEFORE COMPLETING FORM

1. REPORT NUMBER	2. GOVT ACCESSION NO.	3. RECIPIENT'S CATALOG NUMBER
NRL Memorandum Report 4755	AD-A112 545	

4. TITLE (and Subtitle)

APPLICATION OF TIME-RESOLVED SPECTROSCOPIES TO THE STUDY OF ENERGETIC MATERIALS — 1981

5. TYPE OF REPORT & PERIOD COVERED

Interim report on a continuing NRL problem.

6. PERFORMING ORG. REPORT NUMBER

7. AUTHOR(s)

J.M. Schnur

8. CONTRACT OR GRANT NUMBER(s)

9. PERFORMING ORGANIZATION NAME AND ADDRESS

Naval Research Laboratory
Washington, DC 20375

10. PROGRAM ELEMENT, PROJECT, TASK AREA & WORK UNIT NUMBERS

RR-021-02-02; ONR; 65-1192-0-2;
65-1200-0-2; 65-1194-0-2

11. CONTROLLING OFFICE NAME AND ADDRESS

12. REPORT DATE

March 5, 1982

13. NUMBER OF PAGES

66

14. MONITORING AGENCY NAME & ADDRESS (if different from Controlling Office)

15. SECURITY CLASS. (of this report)

UNCLASSIFIED

15a. DECLASSIFICATION DOWNGRADING SCHEDULE

16. DISTRIBUTION STATEMENT (of this Report)

Approved for public release; distribution unlimited.

17. DISTRIBUTION STATEMENT (of the abstract entered in Block 20, if different from Report)

19. KEY WORDS (Continue on reverse side if necessary and identify by block number)

Picosecond
Energetic materials
Lasers

Propellent binders
Fast reactions
Spectroscopy

20. ABSTRACT (Continue on reverse side if necessary and identify by block number)

This report contains a detailed description (including 4 manuscripts) of the research performed as a result of the ONR, and NRL research program (NRL 65-1192).

DD FORM 1473 EDITION OF 1 NOV 65 IS OBSOLETE
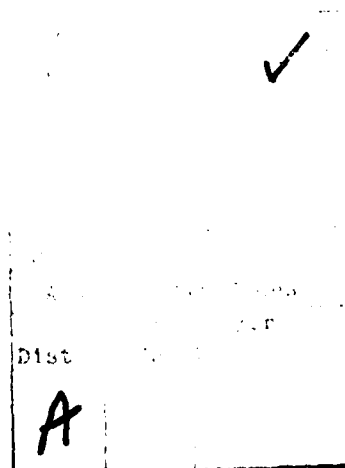S/N 0102-014-6601

SECURITY CLASSIFICATION OF THIS PAGE (When Data Entered)

i/ii

CONTENTS

Dist   A

iii

Application of Time-Resolved Laser Spectroscopies
to the Study of Energetic Materials - 1981

Summary Report

I. Introduction

This report describes recent progress in NRL's research involving the
application of advanced spectroscopies to the study of energetic materials.
This program is currently jointly funded by the Office of Naval Research and
the Naval Research Laboratory as part of their collaborative Special Focus
Program in the area of energetic materials.

The goal of this initial spectroscopic studies are to provide the
appropriate species identification protocols suitable for the study of fast
energetic reactions stimulated by light, heat, and/or shock.

One of the major objectives of this Special Focus Program is to identify
and characterize the important initial stages of energetic reactions as a
function of initiation mode. In order to do this, techniques must be
developed to observe the critical chemical fragments in the required time
scales [e.g. 10^{-11} sec] and to elucidate the kinetics. Using these data
attempts will be made to modify and control the course of the observed
energetic reactions.

The initial species identification experiments have been performed in the
Short Pulse Section of the Optical Probes Branch [Code 6510] at NRL.
Collaboration with the Chemistry Departments of Georgetown University, Johns
Hopkins University and Washington State University, have been quite useful to
the program during the past year.

II. Progress FY 81

The time definition inherent in picosecond pulse excitation enables the
near-instantaneous deposition of energy into the molecular system before
secondary reactions or collisions can occur. As a consequence of the high
optical flux densities obtainable from our short pulse lasers, we can readily
excite molecular systems through either single or multiphoton absorption
processes.

Unimolecular processes are of interest in regard to the determination of
primary photo-induced events. There are many questions about unimolecular
photodissociation which are likely to be answered through the application of
recently developed short pulse techniques. For isolation of specifically

1

unimolecular and early collisional processes, we have been performing experiments on a variety of simple gas-phase organic molecules.   (Table I)

Table I

GASES	EMISSIVE SPECIES/STATES	
CH_3NO_2	C_2	$d^3\Pi_g \quad a^3\Pi_u$; $C^1\Pi_g \quad A^1\Pi_u$
C_2H_2	CN	$B^2\Sigma^+ \to X^2\Sigma^+$
CH_3CN	CH	$A^2\Delta \to X^2\Pi$
CH_2CO	H_α, H_β	Balmer Series
CO	C	$3^1P^o \to 2^1S$
CH_4	C^+	$3^2P^o \to 2^2S$
HCN	O	$3^5P \to 3^5S$; $3^3P \quad 3^3S$

A. Acetylene

Extensive data have been collected for short pulse uv photolysis (25 ps, 266 nm, 10 mJ) of C_2H_2. The dominant emissive fragment product is the carbon diradical, C_2 $d^3\Pi_g$, and its consequent Swan emission ($d^3\Pi_g \to a^3\Pi_u$). The characteristic approaches which we have developed fix upon individual species isolated spectroscopically and detected in emission. Our results have given conclusive evidence that the lowest order process yielding emissive C_2^* is unimolecular and occurs in less than a nanosecond. Streak camera data indicate a grow-in time for this fragment of about 200 picoseconds. The unimolecular nature of the process was confirmed by performing isotopic labeling experiments utilizing mixtures of $^{12}C_2H_2$ and $^{13}C_2H_2$. Emission characteristic of the collisionally produced fragment $(^{12}C\,^{13}C)^*$ was sought, but very little signal attributable to this species was observed at early times of less than a few nanoseconds. After several nanoseconds, a grow in of the $(^{12}C\,^{13}C)^*$ fragment was detected.

Thus C_2^* also is produced intermolecularly from fragments of acetylene in secondary processes that are exhausted within several nanoseconds (~ 7ns at 5 torr). This development must be regarded as fast on the scale of collision rates, although it is readily observed by our instrumentation. The collision partners in this C_2^* formation process appear to be pairs of excited CH^* radicals. Emission spectra from CH $A^2\Pi$ have been observed. These spectra exhibit parent quenching with $k_Q \sim 3 \times 10^{-10}$ sec^{-1}, which is typical for radicals and/or excited electronic states. (Normal molecules give substantially lower rates.) Employing the hypothesis of a collisional formation rate proportional to $(CH^*)^2$ and considering known C_2^* decay rates, the CH^* emission time profiles indicate that these are pertinent rates of precursor exhaustion.

2

B. Carbon Monoxide

C_2 $d^3\Pi_g$ is also formed upon the irradiation of CO with intense picosecond pulses at 266 nm. The processes involved in the formation of C_2 from CO are clearly different from those for other molecules studies, e.g. acetylene, acetonitrile, ketene, methane, etc. There is in fact an extensive literature on related observations of C_2 Swan emission from CO parents. The anomalous features in the emission spectrum, first reported by Fowler some 70 years ago, have attracted repeated spectroscopic and kinetic studies. There has, however, been a deficiency in temporal studies, probably due to lack of instrumental capability.

The most striking feature that is observed is a strong relative enhancement of $V' = 6$ in the Swan spectrum. This is not quite unique to CO, having been also observed in CH_4 and flames. Our time resolved studies reveal that Swan excitation occurs through distinct early and late processes. However, even the early process produces emission protracted far beyond the radiation lieftime of 120 ns. The late process endures for over 20 us and is not affected by pressure. In addition, we have demonstrated that it is the late process which is exclusively responsible for the $V' = 6$ enhancement; the early process yields a vibrational distribution typical of the other parent species listed above.

Our results are consistant with a hypothesis that resonant curve crossing within C_2^* is responsible for $V' = 6$ enhancement; indeed a single-triplet transfer $[^1\Delta_g \to d^3\Pi_g$ may even account for 20 us delays. Protracted chemiluminescence from such a simple parent as CO is quite unusual and was not expected.

C. Acetonitrile

The temporal profiles of fragment emission from CH_3CN have been obtained. Both the C_2 $d^3\Pi_g$ Swan and the CN $B^2\Sigma^+$ Violet Systems have been observed. The populations develop with characteristic pressure dependent formation rates which are linear in pressure and linear in additive methane. Alternative kinetic hypothesis are:

i.   Initial two-quantum excitation of a bound state of the parent, $3^1A''0$, and subsequent predissociation through competing unimolecular and collisional processes.

ii. Prompt scission yielding CN fragments in the ground electronic state $X^2\Sigma^+$ but with very high levels concomitant vibration (a 'dark channel') extending above the emissive B state. This would then be followed by collisional crossing to the B state - essentially an inverse conversion. There is some basis for such an hypothesis in observations and interpetations within the literature and in some observations of our own.

We are currently studying isotopic materials $^{12}CH_3^{13}C^{14}N$, $^{12}CH_3^{12}C^{15}N$, and $^{13}CH_3^{13}C^{14}N$, as well as normal $^{12}CH_3^{12}C^{14}N$. With these compounds we expect to obtain valuable information similar to that found with acetylene. For instance, we believe that the CN fragment derives only from the cyano group of the parent and that the C_2 fragment originates from carbons in the parent methyl groups. Preliminary work with HCN indicates that C_2 is not formed, though CN is abundent.

3

D. Photolysis of Gas-Phase Nitromethane

While the single beam experiments described previously have proven to be
quite fruitful in elucidating processes involving excited-state products, they
provide no information about the non emissive ground-state fragments. These
fragments might well be the major products of the fast energetic reaction
under study. As a consequence, a two-beam excite and probe experiment has
been undertaken during the past year. The experiment utilizes a Nd:phosphate
glass laser system in which the 4th harmonic at 264 nm dissociates the
molecule under investigation and a second beam at 527 nm probes for the
absorption of the fragments utilizing the technique of laser-induced
fluorescence. The laser system was perfected during the past year and has
been applied to study the gas-phase photolysis of nitromethane.

The fluorescence signature of the expected NO_2 fragment was first
determined in NO_2 vapor before attempting the nitromethane photolysis
experiments. The observed fluorescence decay curves could be constructed from
single-exponential fits and were consistant with previously published work on
NO_2. It was found that pressures of > 5 torr nitromethane strongly quenched
NO_2 fluorescence. Therefore, the two beam photolysis experiment was conducted
at pressures between 0.1 and 2 torr.

Nitromethane was then photolysized and probed for ground-state fragments
with the 527 nm pulse. Induced fluorescence was observed which was identical
in spectral and temporal behavior to that observed in NO_2/nitromethane
mixture studies. The formation kinetics of the attributed NO_2 fragment were
investigated by varying the delay time between the 264 nm and 527 nm pulses.
A sharp step in the intensity of the induced fluorescence vs. delay was
observed. The position of the onset and rapid rise in signal appear to
indicate extremely rapid (< 20 ps) formation of the fragment. The fluorescent
signal was found to be linear in UV excitation and probe laser energy
indicating dissociation from the lowest energy $n \rightarrow \pi^*$ transition of
nitromethane.

The papers that have resulted from the work described above are included
in the following pages. In the coming year work will proceed on the
development of the species identification techniques. One technique that
looks particulary promising is the recent development in our laboratory of a
picosecond-white light CARS [coherent-antistokes Raman scattering] technique
in which for the first time an entire Raman spectra can be observed with one
picosecond laser pulse. We are now investigating the applicability of this
technique to the study of energetic reactions.

TIME-RESOLVED C_2 SWAN EMISSION FROM SHORT-PULSE UV FRAGMENTATION OF CO: EVIDENCE FOR TWO C_2 FORMATION MECHANISMS

W.L. FAUST, L.S. GOLDBERG

Naval Research Laboratory, Washington, DC 20375, USA

and

B.B. CRAIG and R.G. WEISS

Department of Chemistry, Georgetown University, Washington DC 20057, USA

We have studied C_2 Swan $(d\,^3\Pi_g \to a\,^3\Pi_u)$ emission resulting from multiphoton UV excitation of CO. Population of $d\,^3\Pi_g$ proceeds through distinct early and late processes, the former giving rise only to normal Swan emission. The late process is responsible for $v' = 6$ enhancement (high-pressure bands), and it dominates time-averaged emission in all bands for >10 Torr of CO.

1. Introduction

The Swan band emission systems of $C_2(d\,^3\Pi_g \to a\,^3\Pi_u)$ are well known for their prominence in flames and appearance under diverse conditions of excitation [1]. C_2 Swan band emission from pulsed excitation of CO includes the high-pressure bands of Fowler [2], now attributed to an enhancement of $v' = 6$. The very identification of the spectroscopic anomalies as components of Swan emission [3] and the peculiar population kinetics [4,5] have afforded challenge to analysis. CO is not entirely unique in producing such features. Several other systems (with parents not necessarily containing oxygen atoms) necessitate distinct reaction schemes. The current understanding of the excess $v' = 6$ population has depended heavily upon high-resolution spectroscopy and term analysis [6,7], and upon potential-curve calculations [8,9]. Although investigated for many years, the origin of the normal and high-pressure Swan emission remains unresolved.

In the current work, we have studied the spectral and temporal development of band and line emission from photolysis products, subsequent to multiphoton 266 nm excitation of CO (5–100 Torr) with a 25 ps pulse. Through signal digitization and averaging, rec-

ords have been obtained over a time scale ranging from a subnanosecond detection risetime to over 50 μs. It is found that excitation of Swan band emission occurs through two distinct mechanisms, *early* and *late*. The high-pressure bands arise only from the late process.

2. Experimental

Excitation was provided by the fourth harmonic of a mode-locked Nd:YAG laser system [10]. The 266 nm single pulse (≈ 10 mJ, 25 ps) was focused into a static gas cell with LiF windows, producing flux densities in excess of 10^{11} W cm^{-2}. Emission was collected at right angles and focused into a Jarrell–Ash 1 m spectrometer (resolution 1 nm). The instrument was coupled at the exit slit to a Varian VPM-154M crossed-field photomultiplier (GaAs, spectral range 200–900 nm, 0.15 ns risetime), or through a side mirror to an EG&G OMA II 500 channel intensified (ISIT) vidicon system. The intensifier section of the vidicon could be gated by a high-voltage pulse generator triggered from the laser pulse. Time-resolved waveforms from the photomultiplier were signal-

5

averaged (e.g. 64 shots) by a Tektronix 7912 AD digitizing oscilloscope (system step-function risetime 0.85 ns) interfaced to a Tektronix 4052 computer. Background and instrumental irregularities were subtracted by use of the computer system, e.g. emission bands generally are represented by the difference between signals at the band head and ≈ 1 nm to the red.

Carbon monoxide was ultra-high-purity grade (Matheson) and was freed of any metal carbonyl contaminants [11]. Pressures were measured by a Wallace Tiernan gauge (± 0.1 Torr). No evidence of changes in the temporal or spectral distribution of emission due to formation of stable photolytic products was observed during a typical series of several hundred pulses (firing rate $\frac{1}{2}$ Hz).

3. Results

3.1. Photolysis spectra — normal Swan and high-pressure features

The Swan bands of $C_2(d\,^3\Pi_g \rightarrow a\,^3\Pi_u)$ present violet-degraded heads (v', v'') spanning much of the visible. Spectral and kinetic observations by others support two classifications for C_2 emission — normal Swan bands associated with $v' = 0$–6, and high-pressure Swan bands associated with an excess population $v' = 6$ [1–7]. Vibrations $v' > 6$ correspond to headless or tail bands which are not evident in any of our current observations. Photolysis of many simple gases (e.g. C_2H_2, CH_3CN, CH_4) yields only the normal Swan bands [10,12]. Fig. 1a is a time-averaged C_2 $\Delta v = +1$ spectrum from 25 Torr of CH_3CN. No exceptional intensity is associated with $v' = 6$. This Swan emission is fully developed very early after excitation (within a few nanoseconds) and persists less than 200 ns [12]. All vibrational-rotational features of these Swan bands share a common time development for a given gas and pressure.

Curves b and c in fig. 1 are time-gated vidicon spectra from 25 Torr of CO. For b, signal was accepted throughout an interval of 900 μs after the laser pulse (so that no emission was rejected) and is typical of reported time-averaged C_2 spectra produced from a CO discharge [6,7]. Swan emission following CO photolysis displays less rotational excitation than is typical of other parent molecules. This effect can be
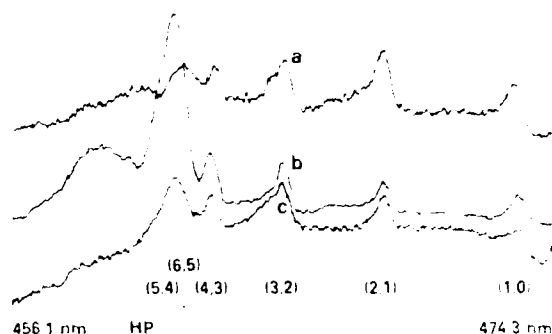
recognized in comparison of figs. 1a and 1b, but it is more evident with better resolution and with baseline subtraction [7,10]. In fig. 1b, the (6,5) high-pressure band is very prominent, 0.18 nm to the red of the (5,4) band head[‡].

For curve c of fig. 1 the intensifier gate was set to accept signal for an interval of 1 μs following the laser pulse. To obtain adequate signal-to-noise within this limited gate interval we accumulated signal from 500 laser pulses. The normal Swan emission is present at this early time, but the high-pressure band is essentially absent. Clearly, there are at least two distinct mechanisms for excitation — an early one developed within ≲ 1 μs and another which assumes importance at later times.

3.2. Time development of spectral features

For illustration of the gross temporal features, figs. 2a and 2b display digital oscilloscope traces recorded at low sweep speed, over a CO pressure range of 15–60 Torr. Here, the normal Swan systems are represented by the intense (0,0) band head at 516.3 nm, which is well isolated. As an example of the high-pressure system we have selected the (6,8) band head at 589.9 nm, which is better isolated than the (6,5) head shown in fig. 1 but is still underlain by a minor

[‡] The band head assignments are taken from the high-resolution work of Meinel and Messerle [7].

v' 6 589.9 nm
60 torr
35 torr
25 torr
15 torr

a

60 torr

HP, v' = 6
Normal, v' 0

c

v' = 0 516.3 nm
60 torr
35 torr
25 torr
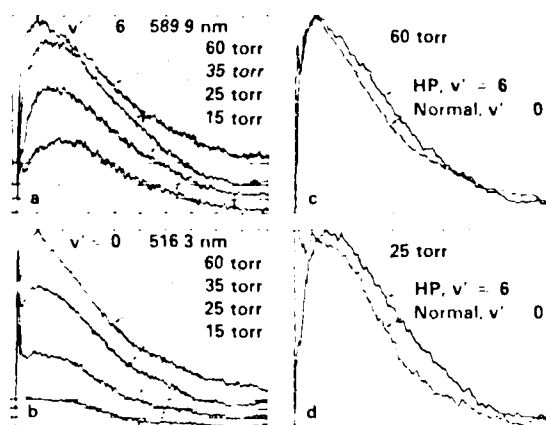15 torr

b

25 torr

HP, v' = 6
Normal, v' 0

d

Fig. 2. Digital oscilloscope traces (signal average of 64 pulses). Comparison of normal and high-pressure C_2 emission profiles at a slow sweep speed (5 μs/div). (a), (b) Demonstration of gross indifference to CO pressure. (c), (d) Overlays to emphasize differences of v' = 6 and v' = 0 emission. For suppression of high-frequency shot noise, the data have been smoothed over 0.7 μs windows.

a 100 ns/div

b 10 ns/div

Fig. 3. Model curves fitting early process emission (v' = 0 at 516.3 nm). 25 Torr of CO. Two limiting τ_2 values (see text) have been employed.

component of rotation attached to normal Swan heads (5,7), etc. The inference from the vidicon spectra of early and late processes is confirmed. For pressures $\geq$ 10 Torr of CO, the late process dominates time-averaged emission i. both the normal Swan and high-pressure bands. Apart from subtle differences of substructure, the duration of the late process is very similar for v' = 6 and v' = 0.

3.2.1. Early process

Figs. 3a and 3b resolve the time development of early Swan emission, (0,0) band head, for 25 Torr of CO. Since the C_2 d $^3\Pi_g$ collision-free lifetime is $\approx$ 120 ns [13], the comparatively slow decay process in fig. 3a reflects not the kinetics of the d $^3\Pi_g \rightarrow$ a $^3\Pi_u$ transition, but rather the destruction of a longer-lived precursor whose lifetime can be expressed simply as $\tau_1 = 1/k_1$ (where k_1 is a pseudo-first-order rate constant representing a sum of the rate constants responsible for loss of the precursor). The rise of the trace in fig. 3b is governed then by the loss of C_2 d $^3\Pi_g$. When the mean pulse energy is changed from $\approx$4 to 12 mJ, the risetime decreases. Hence, at least two processes must be considered to describe the loss of C_2 d $^3\Pi_g$: a bimolecular process (rate constant k_3) to account for
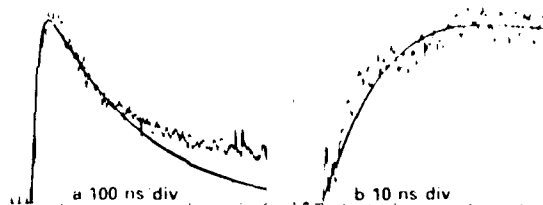
the energy dependence and a pseudo-first-order decay (time constant $\tau_2 = 1/k_2$). k_2 is taken to be linear in CO pressure and to have a zero-pressure limit corresponding to τ_2 = 120 ns. The proposed scheme is outlined by

$$X \xrightarrow{k_1} C_2 \text{ d} ^3\Pi_g . \tag{1}$$

$$C_2 \text{ d} ^3\Pi_g \xrightarrow{k_2} C_2 \text{ a} ^3\Pi_u . \tag{2}$$

$$C_2 \text{ d} ^3\Pi_g + T \xrightarrow{k_3} ? . \tag{3}$$

X represents an unspecified precursor. k_1 and k_2 each represent sums of first-order or pseudo-first-order rate constants describing the overall decay of X and of C_2 d $^3\Pi_g$ respectively. k_3 is the bimolecular rate constant for reactions of C_2 d $^3\Pi_g$ with itself or another transient of similar abundance. The above model allows satisfactory fits to the experimental curves over the range 5–60 Torr, where analysis is feasible. Two analyses were performed for each pressure, representing limits of no quenching (τ_2 = 1.2 × 10^{-7} s [13]) and of strong quenching by CO. As a lower limit for τ_2, we employed a value extrapolated from data for quenching of C_2 d $^3\Pi_g$ by CH$_3$CN [*], according to $\tau_2 = \{(1.2 \times 10^{-7})^{-1} + k_Q [CO]\}^{-1}$ and $k_Q = 7.1 \times 10^5$ Torr^{-1} s^{-1} [12]. These extrema for τ_2, in curve fits to the initial fall of the traces at any given pressure, force no more than 10% change in τ_1. A plot of k_1

[*] We assume that CH$_2$CN is a more efficient quencher of C_2 d $^3\Pi_g$ than CO, since CH$_3$CN contains an unsaturated group similar to CO in addition to three reactive C–H bonds. Thus the k_Q value of CH$_3$CN [12] was adopted as an upper limit.

7

versus CO pressure is near-quadratic ($\tau_1 = 425$ and 60 ns, at 5 and 60 Torr, respectively). At low pressures, the rise and decay curves can be fit adequately without a bimolecular term. In fitting the rise of the transient signal, k_3 is essential at 25 Torr and dominant above 35 Torr. The excitation conditions generate a spatially inhomogeneous concentration of emitting species. A consequence is that no simple significance can be attached to the absolute value of k_3.

3.2.2. Late process

In figs. 2a and 2b, neither the protracted rise nor fall of the emission intensity can reflect the *much* faster $d^3\Pi_g \to a^3\Pi_u$ emission kinetics. Clearly there are intermediate chemical species and/or state(s) of excitation preceding $C_2 d^3\Pi_g$ formation.

Attempts to determine the dependence of the rates on fragment concentrations (hence, pulse-energy dependence) are compromised by the non-specificity of the excitation mechanism together with fluctuations of the laser pulse energy. Nevertheless, with variation of the excitation energy over an adequate range, the energy dependence of emission rise and decay times can be evaluated qualitatively. Such studies show that higher laser energy favors the late process, and the risetime of the late process is independent of pulse energy from ≈ 4 to 12 mJ. A simple kinetic treatment in terms of exponential time constants is not adequate to describe either the rise or the decay of the late process. However, the rate of rise is roughly proportional to CO pressure. The duration of emission from $v' = 6$ and from $v' = 0$ are not greatly different (fig. 2), which may suggest a common intermediate. The decay profiles are complex, though the structure is subtle, and they are not identical for $v' = 6$ and $v' = 0$ (figs. 2c and 2d). The shape features essentially belonging to the decay profile are insensitive to pressure (it must be recognized that the pressure-dependent rate of rise affects to some extent the apparent initial slope of fall).

As mentioned above, the normal Swan $C_2 d^3\Pi_g$ populations produced from C_2H_2 and other simple gases develop rapidly, and they are rotationally hot [6,7,10,14], whereas from CO the time-averaged C_2 spectra are rotationally cold [7,10]. This suggests that for CO in the present study the early process may generate rotationally hot normal Swan emission which is masked on a time-averaged basis by a much
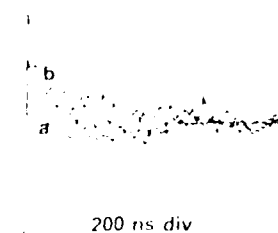
larger rotationally cold population from the late process. In fig. 4, curve a measures the intensity of the (0,0) band head, where the rotational quantum numbers are relatively small. Curve b measures the intensity of associated rotation. There is an excess rotational intensity for the early component of normal Swan emission (curve b), consistent with the above arguments, but the magnitude of the effect is not dramatic.

3.2.3. Other transient species excluded for X

We have identified prompt emission from several other species: the atomic carbon line $3^1P^o \to 2^1S$ (247.8 nm), the C^+ line $3^2P^o \to 2^2S$ (283.7 nm), and the atomic oxygen lines $3^5P \to 3^5S$ (777.3 nm) and $3^3P \to 3^3S$ (844.6 nm). At 25 Torr of CO the C^+ line decays within 4 ns of the excitation pulse; it cannot be directly associated with the rise of C emission at 247.8 nm, which peaks after ≈ 9 ns. The C line shows a non-exponential decay over $\gtrsim 50$ ns, whereas the radiative lifetime is only 2.8 ns [15]. At this pressure, we estimate the formation constant of $C_2 d^3\Pi_g$, τ_1, to be ≤ 270 ns. Consequently, it is impossible for $C 3^1P^o$ to be directly responsible for C_2 production. Similarly, neither $O 3^3P$ nor 3^5P can play a direct role in C_2 formation; the decay constants are ≤ 18 ns at 25 Torr. However, the very appearance of these ionic and excited atomic systems clearly emphasizes the extreme nature of the excitation conditions: production of $O 3^3P$ from $CO X^1\Sigma^+$ requires at least 8 photons at 266 nm (≈ 20 eV). Nevertheless, no components of CO or CO^+ emission were [...]

4 Discussion

The currently favored mechanism for the high pressure emission associates the abnormally high population of C_2 d $^3\Pi_g(v' = 6)$ with a perturbation of the d $^3\Pi_g$ state through a crossing by other electronic states [8,9]. The b $^3\Sigma_g^-$ ($v = 19$) state crosses d $^3\Pi_g(v' = 6)$ at rotational levels of $v' = 19$ and 21 [6]. However, the work of Meinel and Messerle [7], based upon rotational analyses of high resolution spectra, suggests that the $^1\Delta_g$ state could be responsible. Although the details of states and crossers are not firmly established, the mechanistic view is that initially produced higher states of C_2 (C_2^*) lead to abnormally high population of $v' = 6$.

Kunz et al. [16] have proposed a pathway for high pressure emission which invokes C_2O as an intermediate

$$C + CO + M \rightarrow C_2O + M, \qquad (4)$$

$$C_2O + C \rightarrow C_2^* + CO. \qquad (5)$$
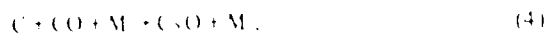
Willis and Devillers [17] have inferred a decay time of 20 µs for the disappearance of a red absorption, which they attributed to C_2O, in 400 Torr of CO. Very similar decay durations ($\sim$ 20 µs) are apparent for each pressure in the emission profiles of fig. 2, and a further experiment at 100 Torr yielded essentially the same result; evidently decay of the intermediate is not dependent upon collisions with the parent. Indeed, the late term temporal profile may actually reflect the production and loss of the same intermediate as that observed by Willis and Devillers.

At the pressures employed here, depopulation of v' levels of d $^3\Pi_g$ should be dominated by quenching from the electronic state (e.g. $\tau_q \approx 20$ ns at 60 Torr). If initially $v' = 6$ were populated exclusively and relaxation to $v' = 0$ were to compete with the quenching process, then the decay profile of $v' = 6$ and $v' = 0$ emission would exhibit in detail the same shape. Figs. 2c and 2d indicate that there are reproducible differences between the shapes of the emission curves from $v' = 6$ and $v' = 0$. Consequently we favor parallel production of $v' = 6$ and $v' = 0$ levels.

5 Conclusion

[...] two distinct populations of C_2 d $^3\Pi_g$ are produced. For > 10 Torr of CO, a late term process is entirely responsible for $v' = 6$ [...] and also dominates the time averaged [...] other vibrational assignments [...] Swan emission. The buildup rate in the time Swan [...] a similar temporal profile. Our data are parallel production of $v' = 6$ and $v' = 0$ [...] room $v' = 6$ [...] C_2 [...] has been identified. The C_2 [...] rotationally hotter than [...] high pressure mechanism at low pressure [...] Swan emission.

References

[1] R.W.B. Pearse and A.G. Gaydon, The identification of molecular spectra (Chapman and Hall, London, 1965).

[2] A. Fowler, Monthly Notices Roy. Astron. Soc. 70 (1910) 762.

[3] G. Herzberg, Phys. Rev. [...] (1946) 362.

[4] D.L. Baulch, A.T. Evans, N.S. Rashidi [...] 411 [...] Opt. Spectry. 2 (1957) 829; D.W. Naegeli and H.B. Palmer, J. Chem. Phys. 48 (1968) 2372, and references therein.

[5] E. Grosse, N. Sadeghi and J.C. Pebay-Peyroula, Chem. Phys. Letters 13 (1972) 557.

[6] J.H. Callomon and A.C. Gilby, Can. J. Phys. 41 (1963) 995.

[7] H. Meinel and G. Messerle, Astrophys. J. 154 (1968) 381.

[8] S.M. Read and J.T. Vanderslice, J. Chem. Phys. 36 (1962) 2366.

[9] K. Kirby and B. Liu, J. Chem. Phys. 70 (1979) 893.

[10] B.B. Craig, W.L. Faust, L.S. Goldberg, P.E. Schoen and R.G. Weiss, in: Picosecond phenomena, Vol. 2, eds. R.M. Hochstrasser, W. Kaiser and C.V. Shank (Springer, Berlin, 1980) p. 283.

[11] W. Braker and A.L. Mossman, Matheson gas data book (1971).

[12] B.B. Craig, W.L. Faust, L.S. Goldberg and R.G. Weiss, to be published.

[13] T.R. McDonald, A.P. Baronavski and V.M. Donnelly, Chem. Phys. 33 (1978) 161.

[14] R. Ineichen and W.C. Nieuwpoort, J. Chem. Phys. 43 (1965) 3680.

[15] D.L. Mickey, Nucl. Instr. Methods 90 (1970) 77.

[16] C. Kunz, P. Harteck and S. Dondes, J. Chem. Phys. 46 (1967) 4157.

[17] C. Willis and C. Devillers, Chem. Phys. Letters 2 (1968) 51.

10

II. EXPERIMENTAL

Much of the apparatus has been described previously [5,6]. Ultraviolet pulses (266 nm, 25 ps) of up to 10 mJ energy were obtained by twice-doubling the amplified single-pulse output from an active-passive mode-locked Nd:YAG laser system. The photolyzing pulse was focused into a static gas sample cell by a quartz lens. A study of the focal region with a bottleneck diode-array pinhole gave a representative beam diameter of 0.15 mm. Emission was directed through a side window and dispersed in a one-meter Czerny-Turner spectrometer. A Varian VPM-154D crossed-field photomultiplier (sapphire window, GaAs photocathode, provided a spectral range 300 – 900 nm, and a risetime 0.15 ns. Waveforms were acquired and averaged, typically for 64 laser pulses, with a Tektronix 7912AD digitizing oscilloscope. The net risetime of the detection system was 1.6 ns. Data were processed with a Tektronix 4052 computer system. An OMA II OMT vidicon also was available for acquisition of time-averaged spectra.

For measurements of emission lifetimes under higher time resolution, we employed an Electrophotonics Model 512 streak camera equipped with an S-20 Photochron II streak tube. The krytron trigger circuitry was modified to reduce sweep jitter. Traces were recorded by a Nuclear Data vidicon system interfaced to a Nicolet minicomputer. To obtain adequate signal levels, color glass filters were used to isolate certain molecular bands. For temporal reference, second-harmonic pulse pairs were provided via a second path to a distinct portion of the streak camera entrance slit. With the sample cell at atmospheric pressure, the first 532 nm pulse was brought into synchronism with the near-instantaneous rise of breakdown emission produced by the 266 nm pulse. The second 532 nm pulse was delivered with a delay set to 500 ps. The streak data were computer-averaged to improve the signal-to-noise of the weak emission. Because of trigger jitter, each streak trace and its corresponding reference were stored individually. The

12

traces were normalized to the response function of the streak camera and video recording system. They were then shifted to a common timing mark and averaged.

Acetylene C_2H_2 was Matheson high-purity grade, further purified by repeated vacuum distillation from liquid nitrogen/n-propanol slush (ca. 148 K) to liquid nitrogen. C_2D_2 was used as supplied by Merck, Inc. The isotopic content of the heavy acetylene was ascertained to be 83.17% C_2D_2 and 16.9% H ^{12}C ^{13}CD; this is based upon an analysis by the supplier of isotopic acetaldehyde prepared from acetylene of the same batch.

13

III. RESULTS

Acetylene at pressures 1 - 10 torr was irradiated under the conditions described above. The triplet C_2 Swan system (430-670nm) was by far the strongest component of emission. Very weak singlet C_2 emission was observed in the Mulliken system $D^1\Sigma_u^+ \to X^1\Sigma_g^+$ (230-240nm) and in the Deslandres-d'Azambuja system $C^1\Pi_g \to A^1\Pi_u$ (360-410nm) [7]. The CH systems $A^2\Delta \to X^2\Pi$ (430-490nm) and $B^2\Sigma^+ \to X^2\Pi$ (314.5nm) were also quite evident. There was no emission from molecular species other than these two diatomics. Molecular continua have been observed in other studies of acetylene photolysis [2,8,9], and continua have been found in our own work with other parents [5,6]. Nevertheless, continuum emission was absent or minimal in the present work with acetylene. Monatomic emission was limited to a few lines; e.g. C (247.6 nm), H (656.3 nm), and C+ (283.7 nm). The integrated intensity for each case was much less than for the diatomics.

A. Detailed Studies of C_2 Swan Band Emission

Figure 1 displays typical oscilloscope waveforms of the $\Delta v = + 1$ Swan emission obtained from 5 torr of $^{12}C_2H_2$, illustrating similar shapes at two vibrational heads and amid rotation. The risetimes are instrumentally limited. These curves were obtained at relatively high excitation energy (ca. 12 mJ). For decay beyond 80% of the maximum, they accept exponential fits with a time constant τ = 45 ns. A plot of $1/\tau$ versus acetylene pressure accommodates a straight line through the zero pressure intercept (τ = 119 ns [9]. The time histories in Fig. 1 therefore represent the residence time of individual C_2 $d^3\Pi_g$ molecules rather than the destruction of some longer-lived precursor (cf. in contrast ref. 10). The slope yields an estimate of the quenching constant of C_2 $d^3\Pi_g$ by C_2H_2, $k_Q = 0.92 \pm 0.1 \times 10^{-10}$ cm^3 s^{-1}.

Streak camera recording allowed a study of the rise of Swan emission with greatly extended time resolution. Since there was essentially no interfering

14

emission, Schott 11-456 and Corning 5-56 filters (in tandem) serve to isolate the $\Delta v = +1$ and $\Delta v = 0$ Swan bands near 474 and 516nm. Fig.2 presents the measured rise of C_2^* emission, from 1 torr of acetylene. The figure includes also two reference pulses and a fit of the rise of Swan emission by a model curve of the form $1 - \exp(-t/\tau)$, with $\tau = 215$ ps. Clearly, collisionless C_2 $d^3\Pi_g$ formation, e.g. unimolecular dissociation, is implied.

To confirm this, we undertook a study of Swan emission from isotopically-labeled C_2H_2 parents. On the basis of spectra from the literature [11], the $\Delta v = +1$ series was selected for our detailed studies, the signal-to-noise and magnitude of isotopic splitting being most favorable. Waveforms were acquired representing emission at increments of 0.2 nm over the range 471.1 to 476.1 nm, encompassing the (1,0) and (2,1) band heads for each of the three isotopic forms. The $^{13}C_2$ (3,2) band head is also present, but it is not effectively resolved from the $^{12}C_2$ (2,1) head. A total pressure of 5 torr was employed uniformly for the single-isotope materials and for a 1:1 $^{12}C_2H_2 : ^{13}C_2H_2$ mixture.

For the mixed-parent gas fills it was immediately apparent that the temporal emission profiles at the band heads of $^{12}C^{13}C$ were not identical in shape to those of the corresponding $^{12}C_2$ and $^{13}C_2$ heads. Qualitatively, the $^{12}C^{13}C$ heads exhibited an excess of emission during an intermediate interval of time, ca. 5 to 25ns after the laser pulse; the asymptotic decays, however, are alike. For a systematic display of this, spectra were constructed as follows: at each wavelength an integral of the emission waveform was taken over an "early" or a "late" interval of time (see Fig. 1; as measured from the laser pulse, early = ca. -2 to +3 ns and late ~ 13 to 42 ns). Such spectra were obtained for laser amplifier settings yielding two values of average uv pulse energy, ca. 7.5 and 12 mJ. In Fig. 3 two of the curves display low-energy early-integral spectra for the distinct parent gases. The third is a similar spectrum for the mixed parents.

15

At this low level of excitation, the early signal associated with the crossed isotope $^{12}C^{13}C$ is relatively small; i.e. the prompt product C_2 largely corresponds to the isotopic parents .

Figure 4 displays, for the equal mixture of parents, the four cases of energy and time interval. The progression of curves from low-energy early to high-energy late confirms the prompt (unimolecular) process asserted above and illustrates also a delayed (collisional) process in which the isotopes are scrambled.

In Figure 5 this point is developed in greater detail, by further manipulation of waveforms (data obtained at 5 torr, with ca. 12 mJ energy). The primary waveform at the wavelength of the $^{12}C^{13}C$ band head, 474.5 nm (curve a of Fig. 5), is not a direct history of the scrambling process: rotation attached to the $^{13}C_2$ band head at 475.3 nm underlies the $^{12}C^{13}C$ band head, and the heavy acetylene is not altogether pure. However, we have developed a procedure effectively to strip out the latter components of signal, employing waveforms at 474.5 nm and 475.3 nm from the heavy-isotope material to establish the relative signal at 474.5 nm due to these components. Curve c in the figure should then represent the collisional production of $^{12}C^{13}C$ due to the joint presence of both parent acetylene isotopes. Waveforms such as c were consistently reproducible. Such data also were gathered and analyzed for 8 torr and 2.5 torr of acetylene. The growing-in time was found to decrease with increasing pressure but was uniformly insensitive to the pulse energy; it is clearly indicated that the risetime is controlled by collisions of a precursor with the parent.

We have noted that the collisional process is unaccelerated at higher pulse energies (Fig.4); it is possible to pursue this same quantitatively. For isotopically-pure parent cases at equal partial pressures, complete scrambling should yield $^{12}C_2$, $^{12}C^{13}C$, and $^{13}C_2$ in abundance ratios 1 : 2 : 1. At 12 mJ, such

16

the collisional C_2 formation is most prominent, all-time integrals were constructed of the excess $^{12}C^{13}C$ signal (Fig. 5, curve c) and of the $^{12}C_2$ signal. The ratio (potentially 2:1) was found to be 1.1:1, corresponding to 70% of total C_2 produced in the collisional process at this relatively high pulse-energy level.

The participation of two processes generating C_2 $^1\Pi_g$, prompt (unimolecular) and delayed (intermolecular), is regarded as established. It has long been recognized that under many conditions Swan emission exhibits high levels of rotational excitation [6,9,10,12]. Thus it is interesting to consider the possibility of distinct degrees of rotational or of vibrational excitation for the prompt and delayed processes generating C_2^*. This question is addressed in Fig. 6, where the data benefit from enhancement of the signal-to-noise ratio inherent in integral spectra. There is no indication of distinct levels of vibrational excitation; but the data points below 473.9 nm, associated with rotational excitation, are uniformly higher for the late-term integrals. Quantitatively, the signal-and-rotation relative to that at the band head is 20% greater for the late time interval. This modest enhancement of rotational excitation for the intermolecular process proved to be quite reproducible. The vidicon is incapable of gating at a speed appropriate for investigation of this issue by temporal separation. However, a spectrum at 25 torr shows more rotation than one at 5 torr; this is consistent with relative enhancement of the collisional process at the higher pressure, and with a higher level of associated rotation for the late collisional process. In a related study of acetylene with 10.6 μ pulses of 250 ns duration [13], a pressure dependence was observed for vibrational as well as for rotational excitation of C_2^* fragments.

Emission associated with high levels of rotation can be observed well to the blue of each band-head region [6,9,...], $\Delta v = +1$. In Fig.7 we compare spectra obtained at 472.4 nm, the 1,0 band head, and at 466.8 nm, all rotation.

17

associated with the entire $\Delta v = +1$ series. The apparent protracted formation of rotationally hot C_2^* reflects a larger fractional contribution of the collisional process, corroborating the inference from Fig. 6 (cf. also Fig. 5, curve c).

B. C_2 Singlet Emission

C_2 possesses a complex structure of electronic states, including singlets and quintets as well as triplets [14]. Several systems of emission are shown [7], among triplet states and among singlets. The systems $C^1\Pi_g \to A^1\Pi_u$ (0,0 at 385.2 nm) and $D^1\Sigma_u^+ \to X^1\Sigma_g^+$ (0,0 at 231.3 nm) were observed, but the integrated intensity for each was $\sim 10^{-2}$ of that in the Swan system. The $D^1\Sigma_u^+$ signal appears within a time less than the instrumental limit of 0.6 ns. There is a delay for the maximum of $D^1\Sigma_u^+$ signal, which suggests a collisional formation mechanism. Each signal decays to 30% of maximum within 25 ns.

It is particularly interesting that McDonald et al. [9], photolyzing C_2H_2 (30 mtorr) with an ArF laser at 193 nm, reported the Phillips system ($A^1\Pi_u \to X^1\Sigma_g^+$, with 3,0 at 771.5 nm and 2,0 at 875.1 nm) to be ca. 10^6 stronger than the Swan system. We did not detect the Phillips system; a careful test led only to an upper bound on the intensity of such emission. A thorough treatment involves several considerations: the $A^1\Pi_u$ emission rate (small), the spectral sensitivity of detection (relatively flat), and the detectivity-threshold (pertaining in our work to instantaneous rather than to time-averaged signal). The finding is that the initial $A^1\Pi_u$ population is no more than 5×10^{-2} of the $d^3\Pi_g$ population; i.e. the relative Phillips population is $\sim 5 \times 10^{-4}$ of that found in the ArF work.

C. CH Emission

In less extensive studies, the rise of emission in the CH A band (0,0 at 431.3 nm) was found to contain two components. At 1 torr there is a prompt rise to 60 % of the peak signal; a further increase occurs within

18

approximately 10 ns. The secondary formation process shows a definite pressure dependence. Unimolecular and intermolecular processes are implied in CH $A^2\Delta$ formation, although we do not have supportive information from labeled isotopes. The curves accept exponential decay with characteristic times of 20 ns at 5 torr and 70 ns at 1 torr, corresponding to $k_Q = 2.8 \pm 0.5 \times 10^{-10}$ cm^3 s^{-1}.

The integrated intensity of the CH C band (0,0 at 314.4 nm) is similar to that of the A band. However, only a prompt component of formation is observed. At 5 torr the emission decays to 30% of the peak within ca. 15 ns. In contrast with the observation of Jackson et al. [15], no emission was observed in the B band (0,0 at 388.9nm) ; the integrated intensity was not greater than 5% of that for the A band.

A. Unimolecular Dissociation Processes

The primary observations here directly establish the existence of a unimolecular dissociation process of acetylene yielding C_2 $d^3\Pi_g$. Such channels also are implied for C_2 $a^3\Pi_g$ and for CH $A^2\Delta$ and $C^2\Sigma^+$. The character and identity of the intermediates remain unresolved and present some challenging questions: e.g., does the process leading to the emissive species [cf. the 215 ps C_2 risetime] represent dissociation from a sufficiently energetic state of the parent manifold, or is there additional excitation [necessarily within the pulse duration] of an intermediate fragment? Also, we must consider the quantum order of the dissociative routes and the role of resonant and nonresonant excitation.

Excitation at 266 nm (4.66 eV, 107 kcal mol^{-1}) is less energetic than the recognized onset of single-quantum absorption in acetylene at 237.7 nm.[16] There is evidence of a triplet state as low as 2.6 to 4.7 eV [17], so that single-quantum excitation cannot be excluded absolutely: for such a transition is both Franck-Condon and spin-forbidden. The uv absorption spectrum of acetylene [18,19] displays the following features in near-coincidence with our $2h\nu = 215$ kcal mole^{-1}: a Rydberg state $\tilde{B}^1$ [212.8 kcal mole^{-1}], and two valence states [213.6 kcal mol^{-1} and F [213.2 kcal mol^{-1}].

We now consider the competing channels for a Franck-Condon $\pi\pi^*$ state at 215 kcal mol^{-1}. Employing high resolution in a search for rotational structure near this energy, Wilkinson found none [18]. This denotes prompt [≤ 1.6 ps] coupling to other states, whether bound [internal conversion to a vibrationally excited ground state or to some other isoenergetic state] or dissociative. The pertinent thermodynamic thresholds for decomposition are [2]: $C_2H + H$, 124 kcal mol^{-1} and $C_2 + H_2$, 144 kcal mol^{-1}. Potential surface calculations [20] and spectroscopic studies [18] have failed to identify a uv state of C_2H_2,

discharges [28], was not observed, nor were there unidentified fragments which might have been assigned to ions. It appears that these are evident only at higher dissociative channels do not demand recognition of essential further features at all (see, however, the discussion of collisional processes in Section IV .

2. Further Excitation of C_2H

The primary two-quantum H elimination from C_2H_2 is at about = 170 nm threshold. There is an ambiguity in the distribution of the excess energy between H atom recoil and the internal energy of the C_2H state generated in this photon excitation. Regardless of the energy content within the reasonable range C_2H^-, absorption of two additional quanta is required to produce the $C_2(d^3\Pi_g, v'=$ ($C_2H + C_2 d^3\Pi_g v' = 6 + H$, 236 kcal mol^{-1}). The $C^1\Pi_g$ requires three additional quanta ($C_2H + C_2 C^1\Pi_g + H$, 221 kcal mole^{-1}). C_2H has been established as a gas-phase photolysis product of C_2H_2 through observation of ESR signals in a rare-gas matrix at 4 K [29]. In a theoretical analysis, Shih et al. [30,31] attribute $\pi \to \pi^*$ excitation to a specific acetylene precursor state, $^1\Sigma_u^+$, leading to $C_2H\ 3^2A'$ and $2^2A''$. The expected (0,0) excitation energy is 6.7 eV or considerably less, very close to the valence states postulated by Wilkinson (who also suggested a π excitation). Absorption [30] and emission [31] of C_2H were treated in extensive ab initio calculations. Excitation of C_2H at 266 nm is supported through $\pi \to \pi^*$ transitions, although the assignment is not complete in detail. Additional resonant absorption leading to further fragmentation (i.e. to C_2^* is then probable. In successive H eliminations, if dissociation occurs through singlet C_2H_2, then doublet C_2H has the appropriate spin to account for the triplet Swan emission; but triplet C_2H_2 would allow either doublet or quartet C_2H.

In other studies of acetylene photolysis [2,8,4] broad structureless continua, tentatively ascribed to C_2H^* or to $C_2H_2^{**}$, have been observed both in absorption and in emission. The bent geometry of the upper C_2H state identified

In the analysis... is entirely consistent with... with the... reported by... These... characteristic... conditions of... strong continuum radiation and the excited... at lower flux.

...

...

3. Considerations of Flux and Fluence in the Excitation Process

The conditions of excitation associated with our experiments are singular. These considerations can be expressed... in terms of flux and fluence, and resonant versus nonresonant transitions. The fluence achieved in the current work at low pulse energy is ca. 10^{17} s^{-1}; this is what was... employed with resonant excitation by pulses of ca. ... in which fragments were detected directly by fluorescence[?] or... spectroscopy [32,33]. The larger (10^4 to 10^{20}) flux values here, ca. 10^{29} s^{-1} cm^{-2}, favor nonlinear excitation through virtual states, ... measure of nonlinear rates nevertheless is small.

Honig et al. [34] gives a rough estimate of the ratio of rates for nonresonant two-photon and resonant single-photon transitions: ... $\approx 10^{-42}$ N_γ, where N_γ is the photon flux in units cm^{-2} s^{-1}. We estimate ... $\approx 10^{-1}$ for the present study.

23

and analysis [...], until near-effective natural lifetimes is encountered [36].

b. Collisional Processes

Collisional [...] [...] [...] [...] has been established. Similar processes seem likely for [...] and [...]. The kinetics of such behavior [...] Fig. 5 suggest that partial depletion of precursor species. This depletion is not necessarily dominated by the process generative of the emissive fragments. In fact, large values of specific quenching constant k are derived even for partners at the full density of the parent [...] for [...], ca. 10 x 10[...] cm³ s⁻¹; and for [...], ca. 30 x 1[...] cm³ s⁻¹. These values are substantially larger than a typical diffusion-controlled rate constant of 1[...] cm³ s⁻¹ [37] and even relatively large even for reactive radical or excited state species [38-40]. Rydberg states or ionic species, affording long-range dipole forces, could account for the large cross sections implied in the observed quenching constants. Alternatively, suprathermal fragment velocities may be involved.

The intermolecular [...] component/accepts poorly a fit to exponential [...] Thus, on an exploratory basis, an hypothesized formation rate proportional to [...]* were used to construct model b^{*} emission profiles. Faster [...] difficult to achieve; nevertheless, the model curves still do not [...] adequately the observed rapid rise.

ACKNOWLEDGMENTS

REFERENCES

1. H. Okabe, J. Chem. Phys. 75, 2772 (1981).

2. H. Okabe, J. Chem. Phys. 62, 2782 (1975).

3. A. H. Laufer, J. Chem. Phys. 73, 49 (1980).

4. L. J. Stief, V. J. DeCarlo, and R. J. Mataloni, J. Chem. Phys. 42, 3113 (1965).

5. B. B. Craig, W. L. Faust, L. S. Goldberg, R. G. Weiss, and R. H. Lehmberg, Picosecond Phenomena, Vol. 2, eds. R. M. Hochstrasser, W. Kaiser, and C. V. Shank, Proc. 2d Int'l Conf. on Picosecond Phenomena, Cape Cod, Mass. USA, June 18-20, 1980, Springer-Verlag, Berlin 1980, p. 253; see also references therein.

6. B. B. Craig, W. L. Faust, L. S. Goldberg, R. H. Lehmberg, R. G. Weiss, and R. G. Weiss, Fast Reactions in Energetic Systems, eds. C. Capellos and R. F. Walker, Proc. NATO Adv. Study Inst. Preveza, Greece, July 1-11, 1980, D. Reidel Publ. Co., Dortrecht Netherlands 1981, p. 413.

7. R. W. B. Pearse and A. G. Gaydon, Identification of Molecular Spectra, Chapman and Hall, London 1965.

8. K. H. Becker, D. Haaks, and M. Schurgers, Z. Naturforsch. 26A, 1770 (1971).

9. J. R. McDonald, A. P. Baronavski, and V. M. Donnelly, Chem. Phys. 33, 161 (1978).

10. B. B. Craig, W. L. Faust, L. S. Goldberg, and R. G. Weiss, Chem. Phys. Lett. 83, 265 (1981).

11. R. K. Dhumwad and N. A. Narasimham, Can. J. Phys. 46, 1254 (1968).

12. W. Lochte-Holtgreven, Z. fur Physik 64, 443 (1930),

13. J. H. Hall, Jr., M. L. Lesiecki, and W. A. Guillory, J. Chem. Phys. 68, 2247 (1978).

14. H. Kinny and R. Liu, J. Chem. Phys. 70, 783 (1979).

15. W. M. Jackson, J. B. Halpern, and C. S. Lin, Chem. Phys. Lett. 55, 254 (1978).

16. G. B. Kistiakowsky, Phys. Rev. 37, 276 (1931).

17. G. W. Barton and H. B. Dunnicker, J. Chem. Phys. 37, 468 (1962).

18. P. G. Wilkinson, J. Mol. Spectr. 2, 387 (1958).

19. H. Okabe and K. Watanabe, J. Chem. Phys. 40, 390 (1964).

20. P. Brodtlin, Chem. Phys. 11, 329 (1975).

21. A. H. Lauter and A. M. Bass, J. Phys. Chem. 83, 310 (1978).

22. Note that fluorescence is not ordinarily observed from acetylene. There is
such a report for acetylene in an inert gas matrix: L. E. Brus,
J. Mol. Spectr. 75, 245 (1979).

23. K. Evans, R. Scheps, S. A. Rice, and D. Heller, Chem. Soc. Faraday Trans. II,
856 (1973).

24. W. L. Hase and Da-Fei Feng, J. Chem. Phys. 61, 4690 (1974).

25. C. S. Sloane and W. L. Hase, J. Chem. Phys. 66, 1523 (1977).

26. V. E. Bondybey, J. A. Miller, and H. C. McCulloh, J. Chem. Phys. 69, 298
(1978).

27. J. Kuelke, A. Schweig, and W. Thiel, Chem. Phys. Letters 79, 547 (1981).

28. A. E. Douglas and J. R. Morton, Astrophys. J. 131, 1 (1960).

29. W. R. M. Graham, K. I. Dismuke, and W. Weltner, Jr., J. Chem. Phys. 60, 3817
(1974).

30. S. Shin, S. D. Peyerimhoff, and R. J. Buenker, J. Mol. Spectr. 64, 167 (1977).

31. S. Shin, S. D. Peyerimhoff, and R. J. Buenker, J. Mol. Spectr. 74, 124 (1979).

32. J. Tusee and R. B. Bernstein, J. Chem. Phys. 71, 1369 (1979).

33. S. Koenl, H. J. Neusser, and E. W. Schlag, J. Chem. Phys. 72, 4327 (1980).

34. S. Honig, J. Jortner, and A. Szoke, J. Chem. Phys. 46, 2714 (1967).

35. This support is afforded by measurements of emission intensity versus laser
pulse energy, executed in the current work; the largest power-law exponent
was 1.6.

36. A very interesting indication of bottleneck effects may be found in the
observations of Neusser et al. [33], upon photolysis of benzene. After an initial
infrared excitation, the primary ir pulse was ineffective toward subsequent
fragmentation, but a parallel or following visible pulse was quite effective.

37. V. N. Kondratiev, Chemical Kinetics of Gas Reactions, Pergamon Press, N.Y.,
1964; s. Ch., p. 354.

38. A. H. Zewail, D. E. Cooper, T. E. Orlowski, and J. R. Bergener, Rev. Phys. Letters
43, 190 (1979).

39. M. W. Bosnali and D. Perner, Z. Naturforschung 26a, 1768 (1971).

40. A. P. Baronavski and J. R. McDonald, Chem. Phys. Letters 56, 369 (1978).

41. L. Pasternack and J. R. McDonald, Chem. Phys. 43, 173 (1979).

42. V. M. Donnelly and L. Pasternack, Chem. Phys. 39, 427 (1979).

43. M. N. R. Ashfold, M. A. Fullstone, G. Hancock, and G. W. Ketley, Chem. 55, 245 (1980).

44. C. K. Luk and R. Bersohn, J. Chem. Phys. 58, 2153 (1972).

45. W. M. Jackson, J. Chem. Phys. 61, 4177 (1974).

EARLY INTERVAL   LATE INTERVAL
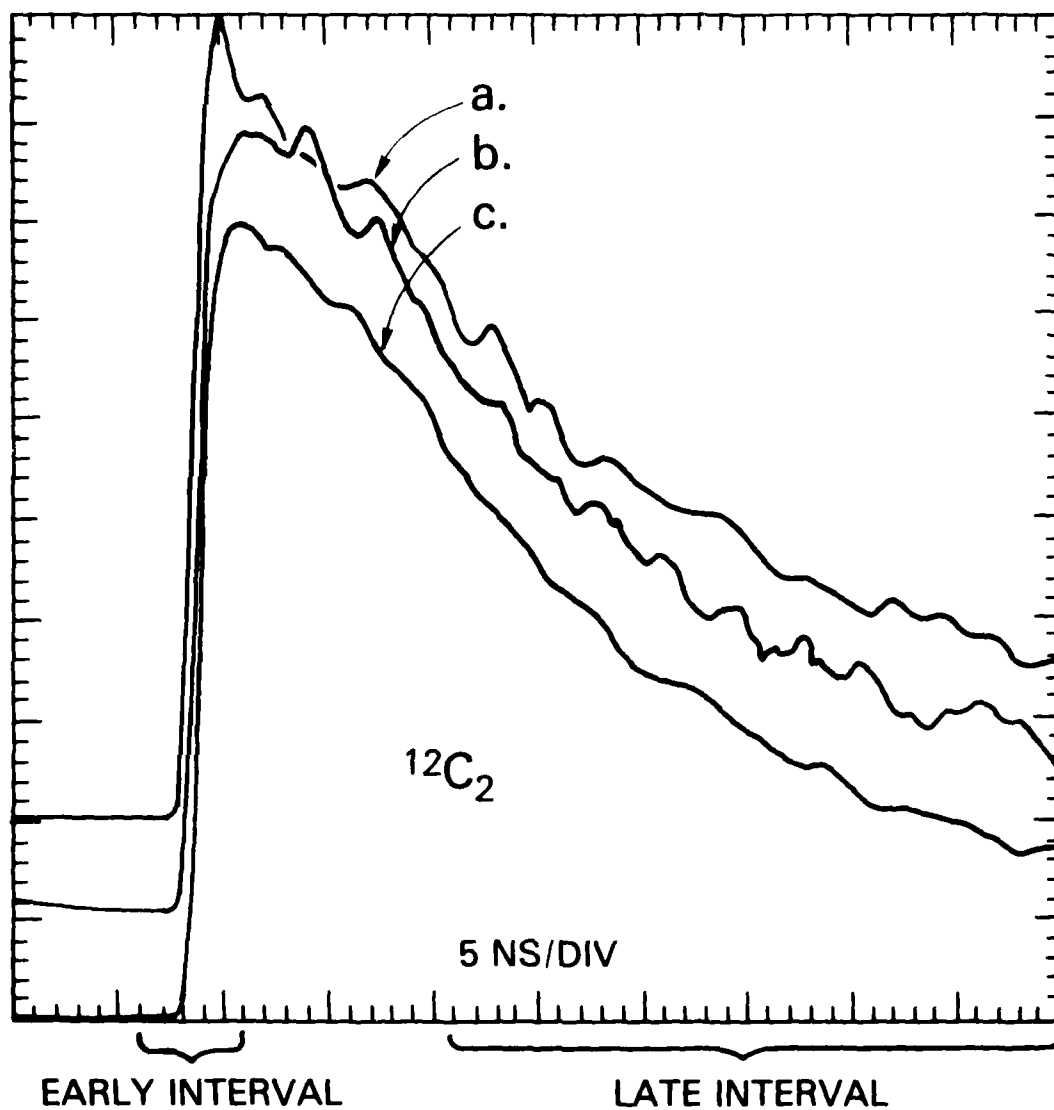
Figure 1

Comparison of temporal profiles for C_2 Swan emission at band heads and arid rotation; averages of 64 pulses.

The curves have been scaled to equal peak heights.

5 torr of $^{12}C_2H_2$; the same total pressure pertains for each figure.

uv pulse energy ca. 12 mJ.

a) (1,0) band head at 473.9 nm.
b) Rotation associated with the (1,0) head, at 472.7 nm.
c) (2,1) head at 471.7 nm.

31
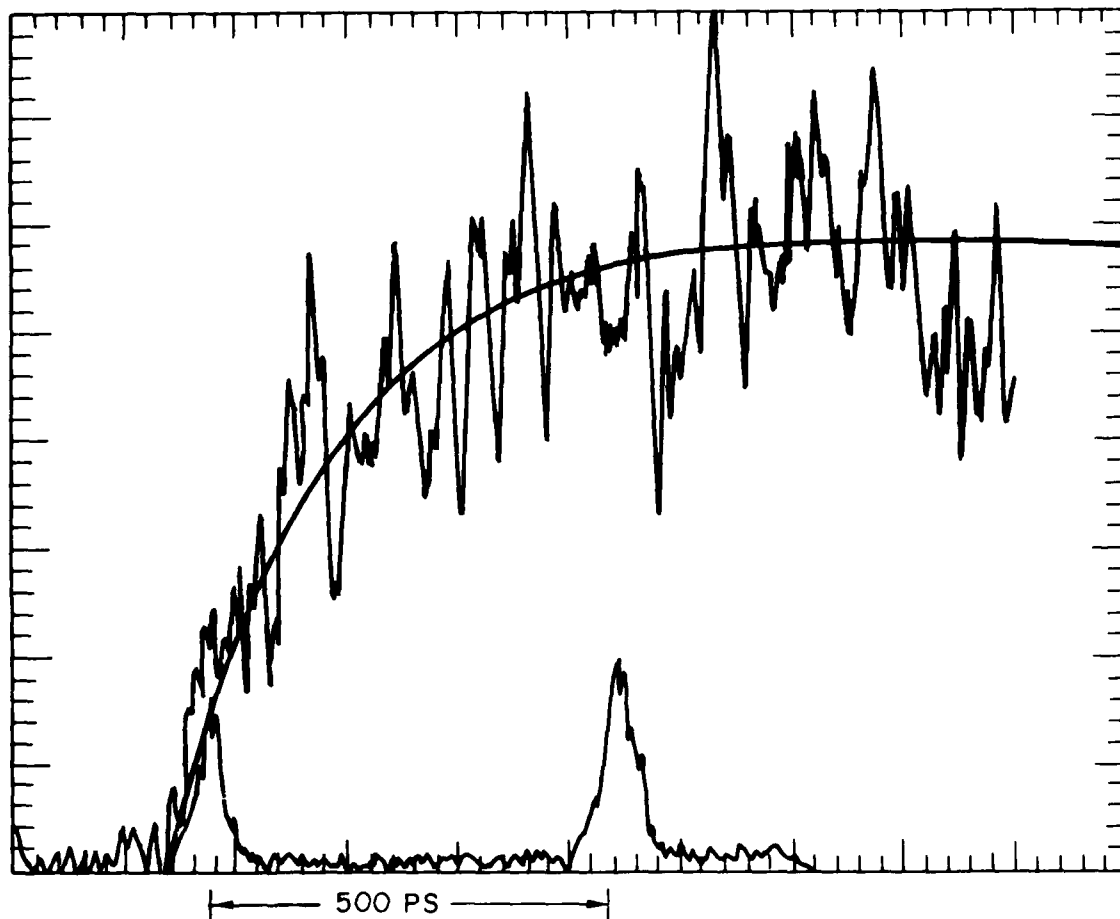
Figure 2

Streak camera record of the rise of Swan emission in the $\Delta v = +1$ and $\Delta v = 0$
bands; the average of 10 pulses.

Also shown are a model curve with time constant 215 ps, and second-harmonic
reference pulses at a pair separation of 500 ps.
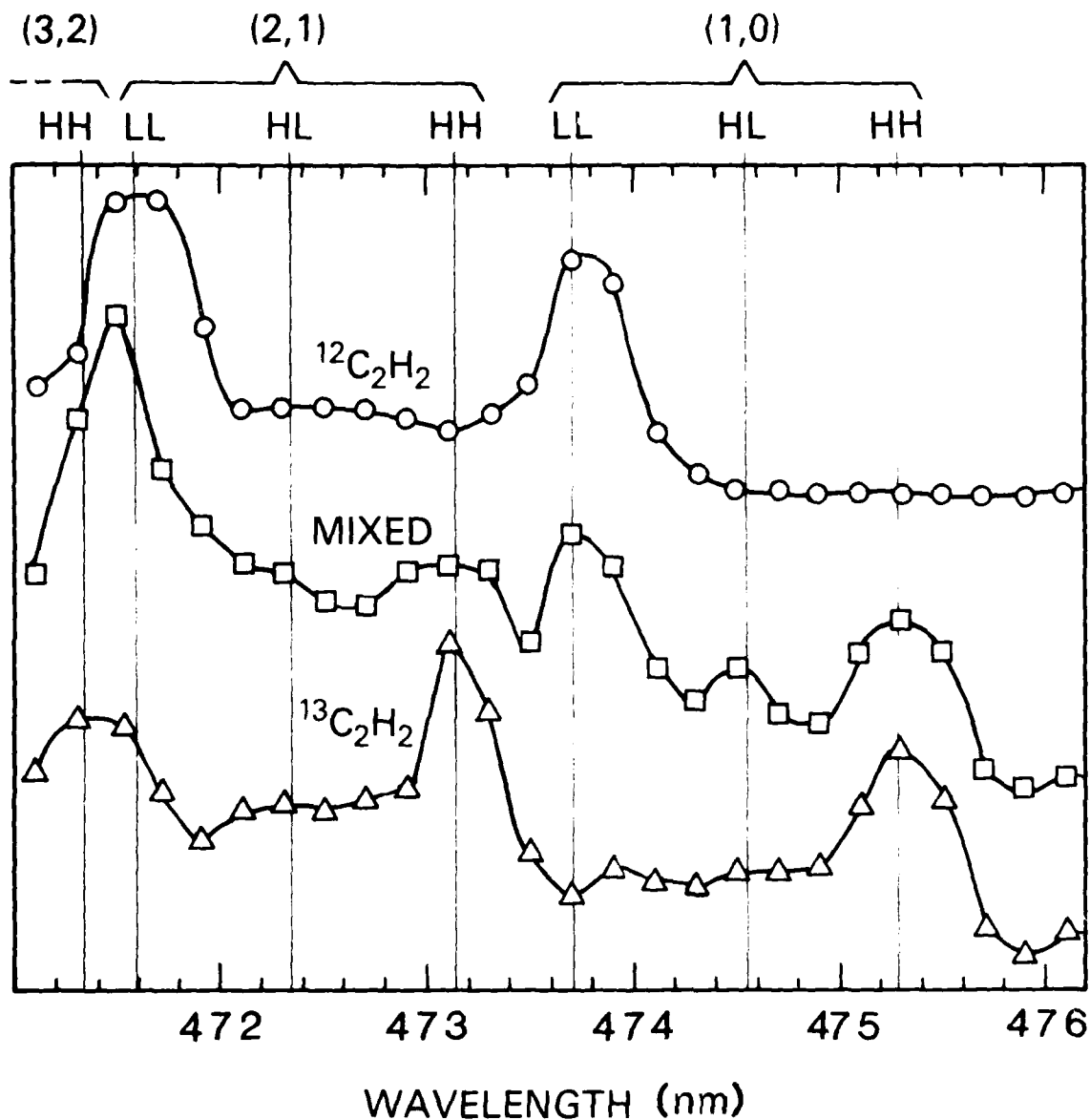
Figure 3

Spectra of early emission (first 5 ns; see Fig. 1) in the C_2 $\Delta v = +1$ Swan series; uv pulse energy ca. 2.5 mJ.

Curves for isotopically-distinct parent acetylenes, and for a 1:1 mixture of $^{12}C_2H_2$ and $^{13}C_2H_2$.

The notations HH, HL, and LL attached to band heads refer to heavy and to light isotopes of carbon.
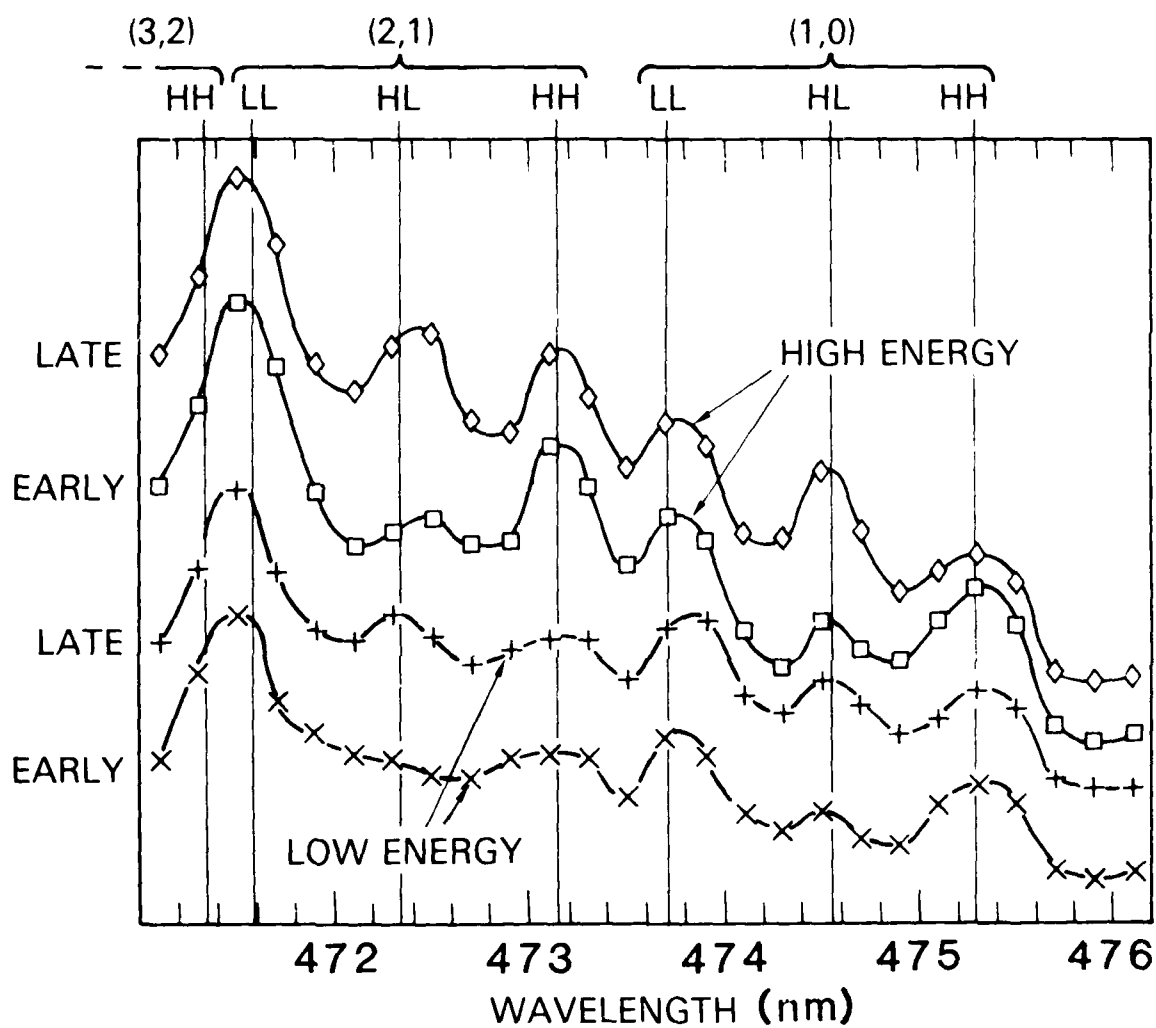
Figure 4

Spectra of Swan emission ($\Delta v = +1$) within early and within late intervals of time (see Fig. 1); curves for uv pulse energies ca. 2.5 mJ and ca. 12 mJ.

1:1 $^{12}C_2H_2$:$^{13}C_2H_2$ mixture.

34

5 NS/DIV

Figure 5

Construction of the time history of Swan $^{13}C^{13}C$ arising in the collisional process; uv pulse energy ca. 12 mJ.

1:1 $^{13}C_2H_2$:$^{12}C_2H_2$ mixture.

a) Primary record of emission at the $^{13}C^{13}C$ (1,0) head, 474.5 nm.
b) Reference waveform obtained by appropriate scaling of the emission record at the $^{13}C_2$ (1,0) head, 475.3 nm.
c) Subtraction of curve **b** from curve **a**, representing collisionally-formed $^{13}C^{13}C$.

35
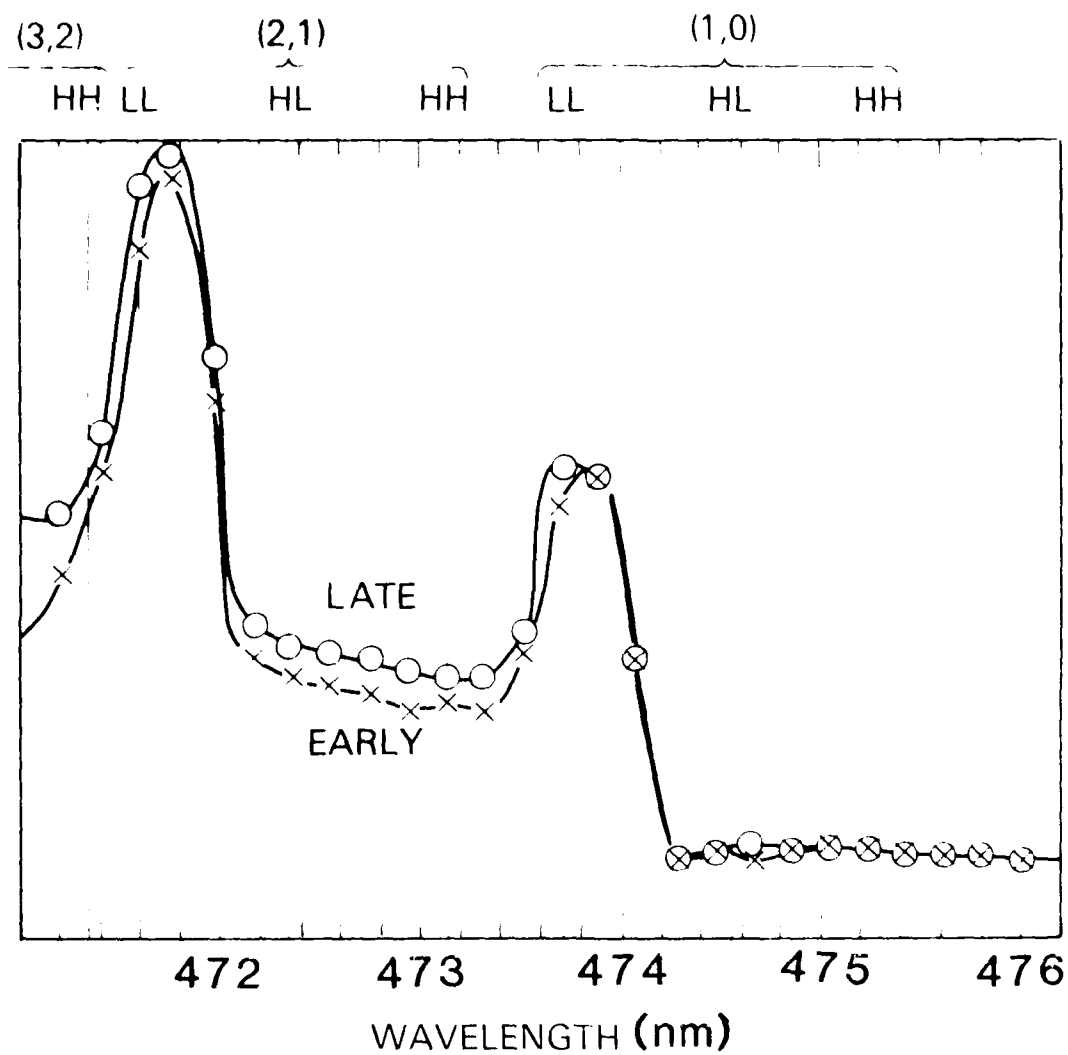
Figure 6

Comparison of vibrational/rotational distributions for early and late C₂ d³Πᵤ
populations, Δv = +1 series; uv pulse energy ca. 12 mJ.

5 NS/DIV
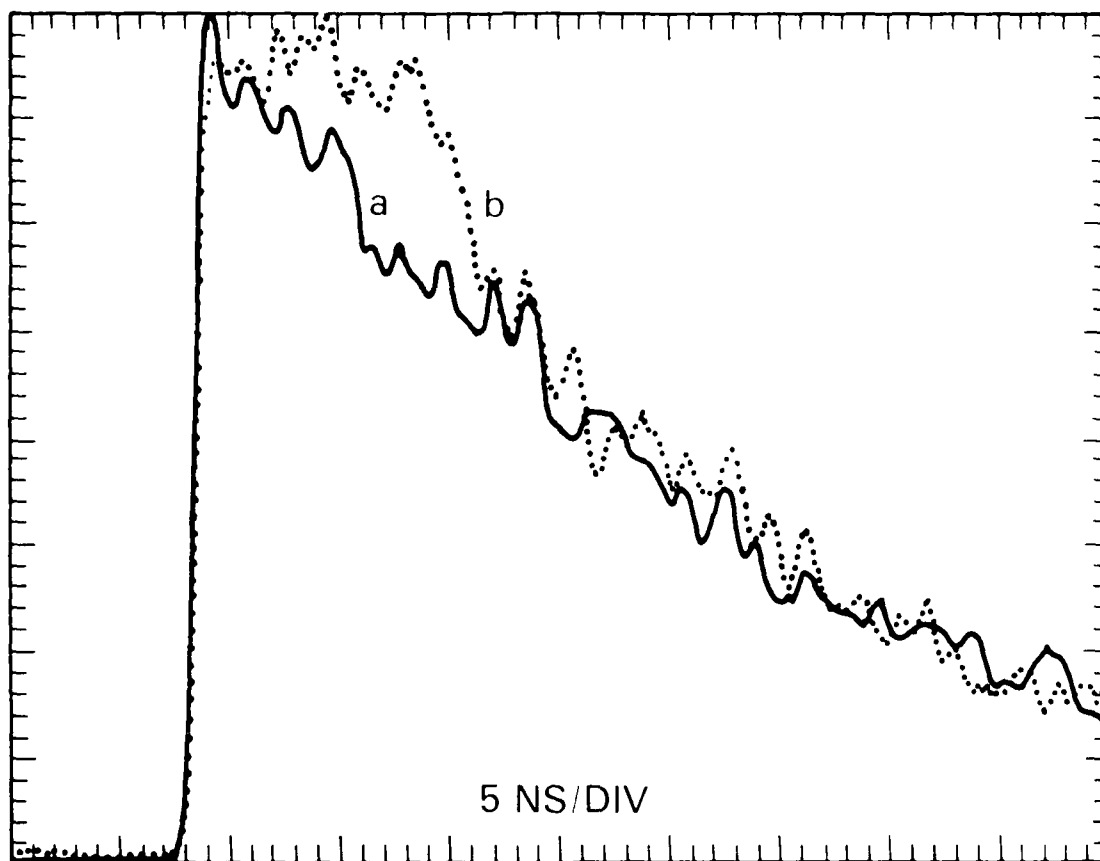
Figure 7

Comparison of temporal profiles for C_2 Swan emission amid states of high rotation and at a band head.

The curves have been scaled to a common late-term signal level.

a) 473.9 nm, the (1,0) band head.
b) 462.8 nm, hot rotation.
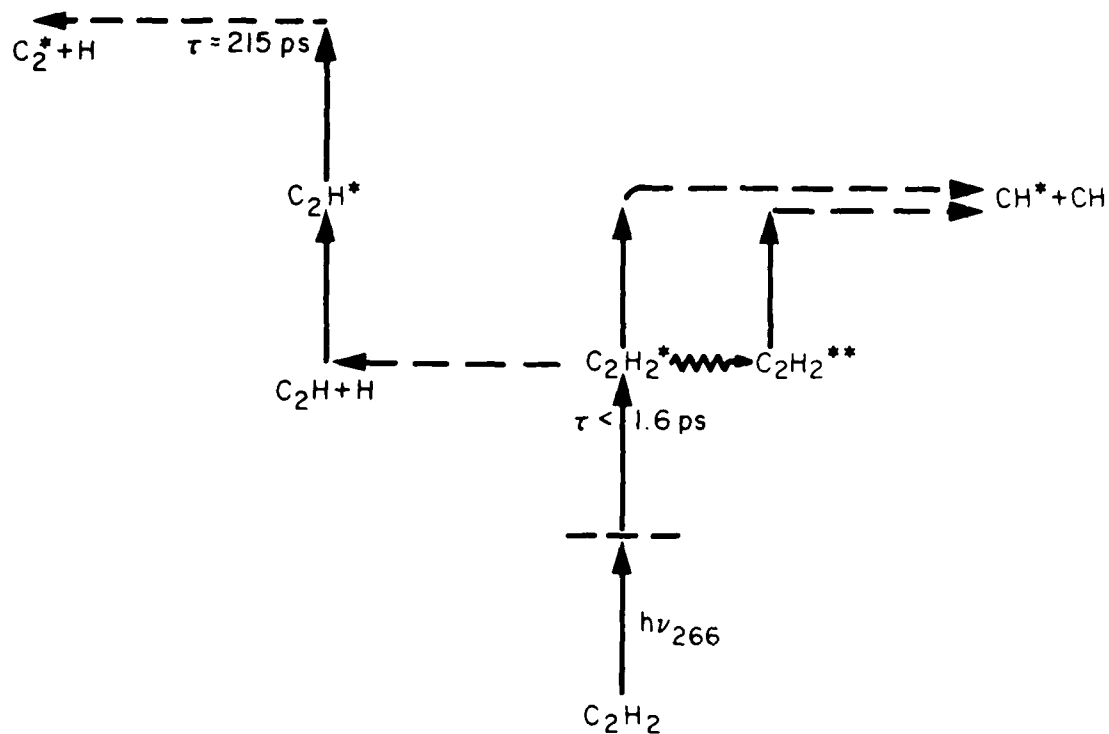
Figure 8

Schematic of preferred channels of $\pi \rightarrow \pi^*$ excitation (vertical arrows), intramolecular relaxation (wavy arrow), and unimolecular fragmentation (dashed arrows) for photolysis of C_2H_2 by 266 nm 25 ps pulses.

38

Picosecond UV Photolysis and Laser Induced Fluorescence

Probing of Gas-Phase Nitromethane*

by

P. E. Schoen, M. J. Marrone, J. M. Schnur, and L. S. Goldberg

ABSTRACT

In a dual-beam picosecond experiment, we have performed UV photolysis
of gas-phase nitromethane and have monitored the subsequent evolution of the
NO_2 fragment population by laser induced fluorescence. The NO_2 radicals are
formed promptly, within the ~ 5 ps pulse resolution of the experiment. Their
population remains roughly constant for a probe delay time extending to 20 ns.
The fluorescence intensity depends linearly upon both the photolyzing and the
527 nm probe pulse energies. The photolyzing 264 nm pulse itself generates
some NO_2 in an excited fluorescing state.

The UV photolysis of nitromethane has been studied extensively for many years [1-9]. A number of authors have inferred, generally on the basis of chemical analysis of final products, that the primary photodissociation process leads to formation of the free radicals CH_3 and NO_2. However, identification of these fragments has been difficult because of their high reactivity. The first direct evidence for their presence among the photolysis products of nitromethane was provided by the electron paramagnetic resonance experiments of Bielski and Timmons [3]. Colles et al. utilized opto-acoustic detection to provide the first spectral identification of the NO_2 fragment from continuous photolysis of nitromethane [7]. More recently, laser techniques using UV [8,9] and multiphoton IR [10,11] excitation have led to the generation and detection of the NO_2 fragment. In the case of UV laser photolysis in the gas phase, Spears and Brugge observed vibrationally excited NO_2 fragments by means of laser induced fluorescence (LIF) on a microsecond time scale [8]. However, experiments by Kwok, et al., employing nano-second laser photolysis and mass spectroscopic fragment detection techniques observed no photodecomposition products [12].

In this letter, we report the first direct observation on a picosecond time scale of fragment formation in the UV photolysis of gas-phase nitromethane. Using a dual-beam experiment with LIF probing, we have determined that NO_2 fragments, identified from their fluorescence spectrum and quenching kinetics, are generated promptly by the UV excitation, within the 5 ps pulse resolution of the experiment.

This supports assignment of the observed reaction as:

$$CH_3NO_2 \xrightarrow{h\nu} CH_3 + NO_2 \qquad\qquad (I)$$

Experiment

Our nitromethane samples were obtained from Baker reagent grade material, which we distilled under nitrogen, collecting the middle fraction, b.p. 101 – 102°C. Individual samples were degassed by several freeze/thaw-vacuum pumping cycles. Samples of 0.1 to ~ 3.0 Torr pressure were loaded into a 15 cm diameter stainless steel cell whose interior walls had been coated with black Teflon to reduce scattered light. The entrance and exit cell windows were of lithium fluoride, and internal baffling was provided to prevent window fluorescence induced by the laser pulses from reaching the photodetector. Light emitted at 90° from the laser path was collected by a lens and focused through long-wavelength-pass color filters onto a slit in front of an EMI 9658 phototube. The tube had an S-20 photocathode (red sensitive to ~ 900 nm) and a pulse response (FWHM) of ~ 20 ns. The signal was processed by a Tektronix 7912AD digitizing oscilloscope coupled to a Tektronix 4052 computer for time integration of waveforms, and for data manipulation and storage.

The laser was a passively mode-locked Nd:phosphate glass oscillator/amplifier system [13] which generated 1054 nm single pulses typically of 5 ps duration and ca. 25 mJ energy at a repetition rate of 1/5 Hz. The IR pulse was frequency-doubled twice to give a photolyzing UV pulse energy of up to 3 mJ at 264 nm. The residual IR pulse energy was separated from the direct laser path by a beam splitter and was frequency-doubled independently, to give a probe pulse of up to 10 mJ at 527 nm. The probe pulse was directed along an optical delay line, and subsequently recombined co-axially with the photolyzing pulse. Both pulses were then sent into the sample cell without focusing, giving a photolyzing beam diameter of ~ 4 mm. Pulse energies were recorded on each shot, and were used to normalize the observed sample fluorescence data. The temporal and spectral quality of the pulses were monitored as the experiment

progressed by a two-photon fluorescence cell/vidicon and by a 0.5 meter
spectrograph/Reticon array.

The zero time delay between the UV and probe pulses was determined by a
photobleaching measurement in which the two pulses were focused into a thin
cell filled with rhodomine 6 G dye solution. The UV pulse depopulated the
dye ground state sufficiently that a weak probe pulse arriving after the UV
pulse was transmitted.

Results

Figure 1 shows two representative traces of fluorescence intensity versus
time, averaged over 8 laser shots, for a nitromethane pressure of 1.2 Torr.
The lower trace shows the fluorescence signal for the UV photolyzing pulse
alone. The upper trace was generated by a UV pulse plus a 527 nm probe pulse
delayed by ~ 200 ps. A probe pulse alone produced virtually no signal either
initially or after hundreds of UV shots into the cell. The emission in Fig. 1
was filtered by a Corning 2-73 filter, which transmits wavelengths longer
than ~ 560 nm. While the UV pulse itself obviously produces a fluorescing
fragment, input of the 527 nm pulse has increased the fluorescence intensity
roughly 3-fold. The observed fluorescence has a risetime that is phototube-
limited; its decay shows a single exponential fall time which is strongly
dependent on gas pressure. The decay time for the UV-only case is roughly the
same as that for UV + probe. The integrated fluorescence intensity reaches a
maximum at about 10 Torr. of nitromethane, but the quenching rate at this
pressure is too fast to be resolved with our phototube.

The collision free (< 1 m Torr) lifetime reported for NO_2 fluorescence is
approximately 55 µsec [14]. At our lowest nitromethane pressure of
~ 100 mTorr observe a decay time of ~ 1.5 microseconds. The emission is more
rapidly quenched at still higher pressure; at 2.2 Torr the decay time was
~ 70 ns. A Stern-Volmer plot of decay rates versus pressure is linear over
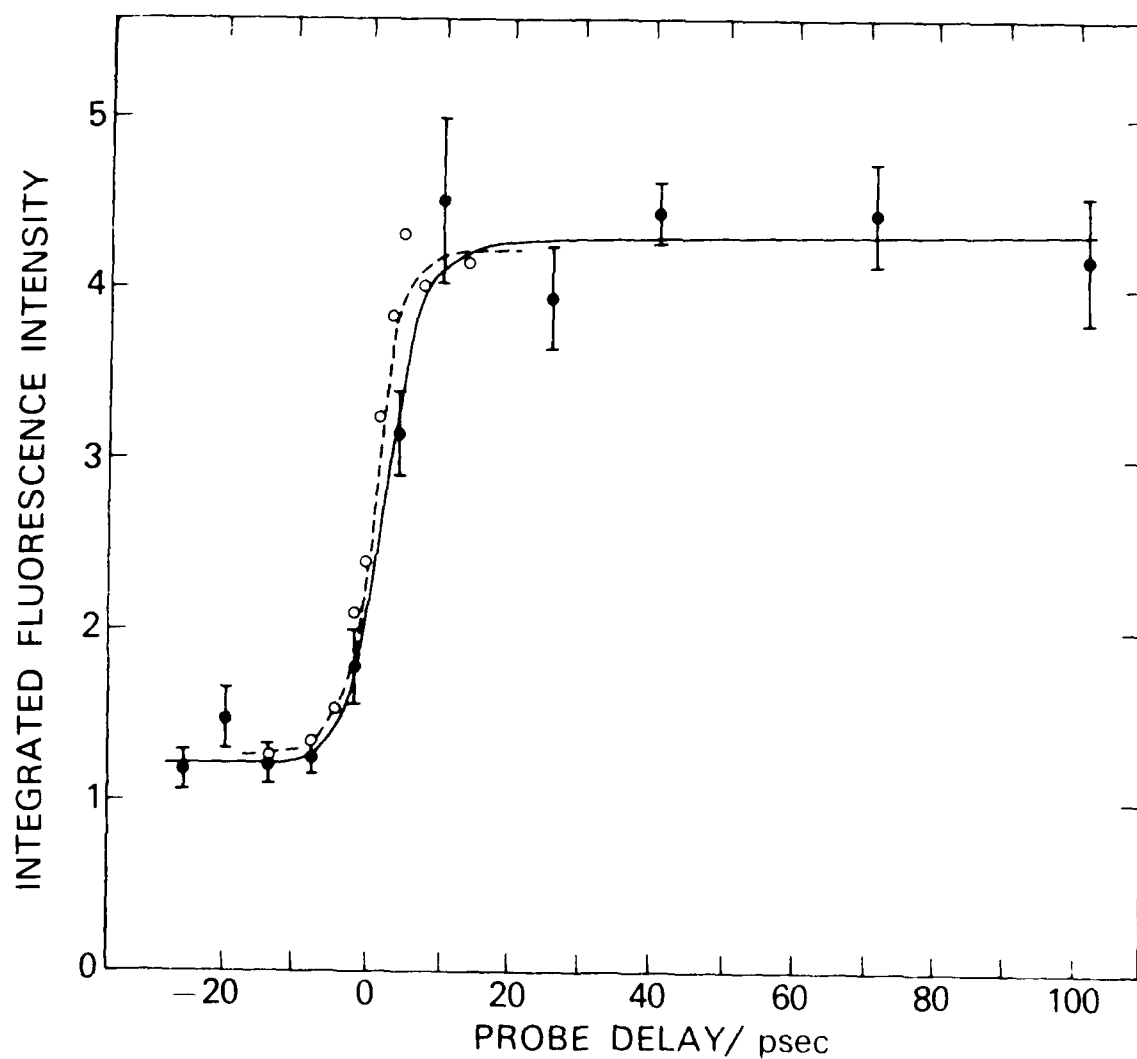
Fig. 1 - Fluorescence from photolyzed nitromethane at a pressure of 3.5 torr. Lower trace shows emission resulting from a single 5 psec pulse of 264 nm UV light; upper trace shows emission produced by UV irradiation followed after a 200 psec delay by a 527 nm probe pulse. Emission is filtered in both cases with a Corning 3-73 filter which transmits wavelengths > 460 nm.

the pressure range of our experiment, indicating the collision-free lifetime of the emitting species is long. This is qualitatively consistent with the known quenching behavior of NO_2 in various gases [15].

Although the fluorescence signal intensity was too weak to yield a spectrum, use of a sequence of long-wavelength-pass filters indicated that in the region from the probe wavelength to ~ 750 nm the probe-induced emission was broad and featureless. No significant emission signal was observed on the antistokes side of the probe wavelength. Thus the spectral characteristics and long lifetime of the emitting species are clearly consistent with NO_2.

We performed a series of experiments to determine the power-law dependence of the fluorescence. Fig. 2 shows a log-log plot of the time-integrated fluorescence intensity as a function of UV pulse energy, for individual laser shots. The lower curve shows the UV + probe induced fluorescence, normalized by probe pulse energy. The upper curve shows UV-only induced fluorescence. Both curves exhibit a unit slope extending over almost 2 decades in UV energy, indicating an effect linear in excitation pulse energy. Since the energy of the photolyzing photon is ~ 4.7 ev and C-N bond cleavage requires ~ 2.6 ev [17], the excess energy for single UV photon induced photolysis should yield fluorescence only at wavelengths longer than ~ 575 nm. This agrees with our observations.

A variable time delay was introduced between the UV and probe pulses to determine whether there was a measurable induction period between excitation of the nitromethane molecules and the appearance of NO_2 fragments. The results shown in Fig. 3 indicate that the population of ground state NO_2 probed by the 627 nm pulse appears and rises to a plateau within the ~ ps pulse resolution of the experiment. For delay times as long as ~ , the height of the plateau remains approximately constant. In addition the results unaffected by changes in nitromethane pressure. Each point in Fig. 3 repre-

44
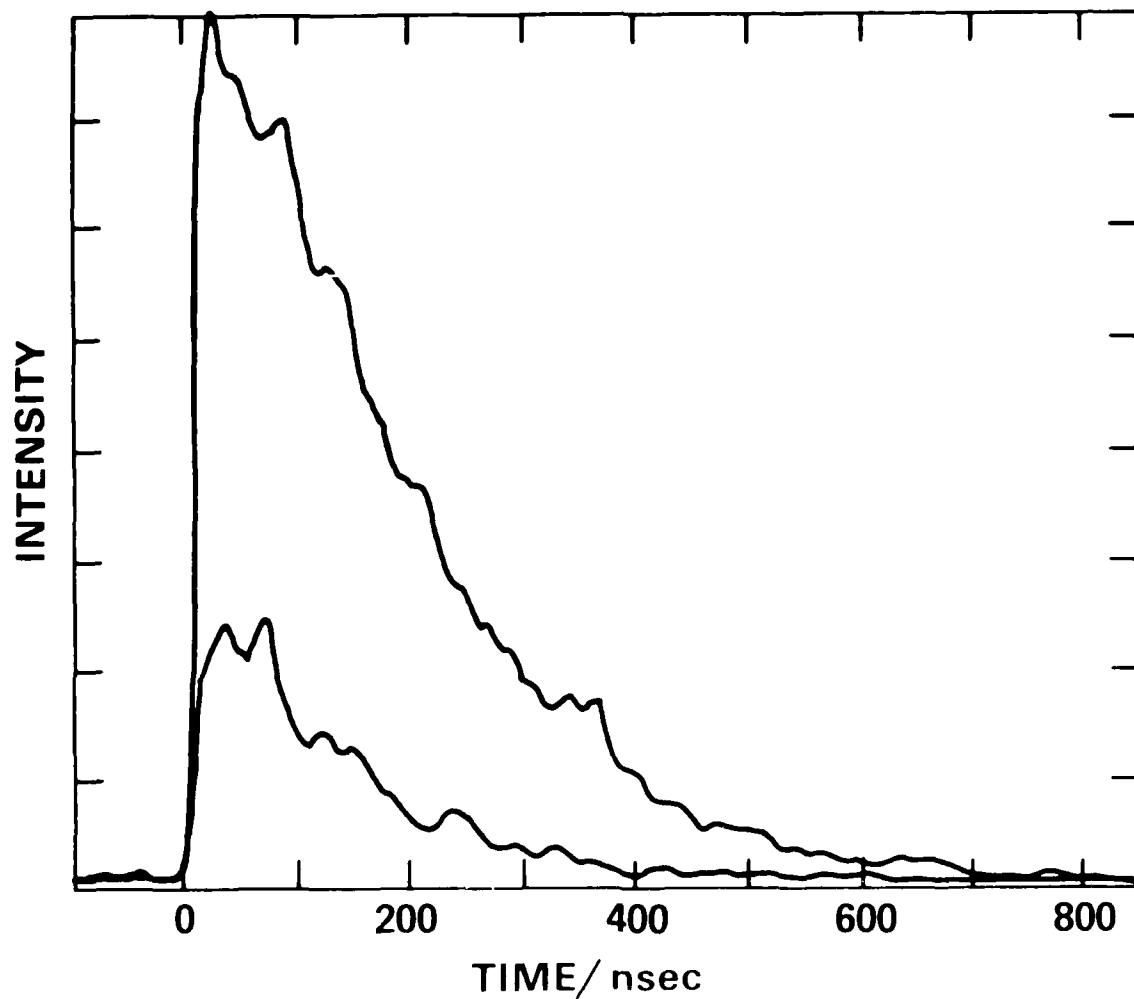
Fig. 9 - Fluorescence power-law dependence in nitromethane photolysis: time-integrated fluorescence signal versus UV excitation pulse energy. Upper trace: Fluorescence caused by UV-only excitation. Lower trace: Fluorescence caused by UV + probe irradiation, normalized to probe pulse energy. Probe time delay was 1 nsec. Nitromethane pressure was 0.2 Torr.
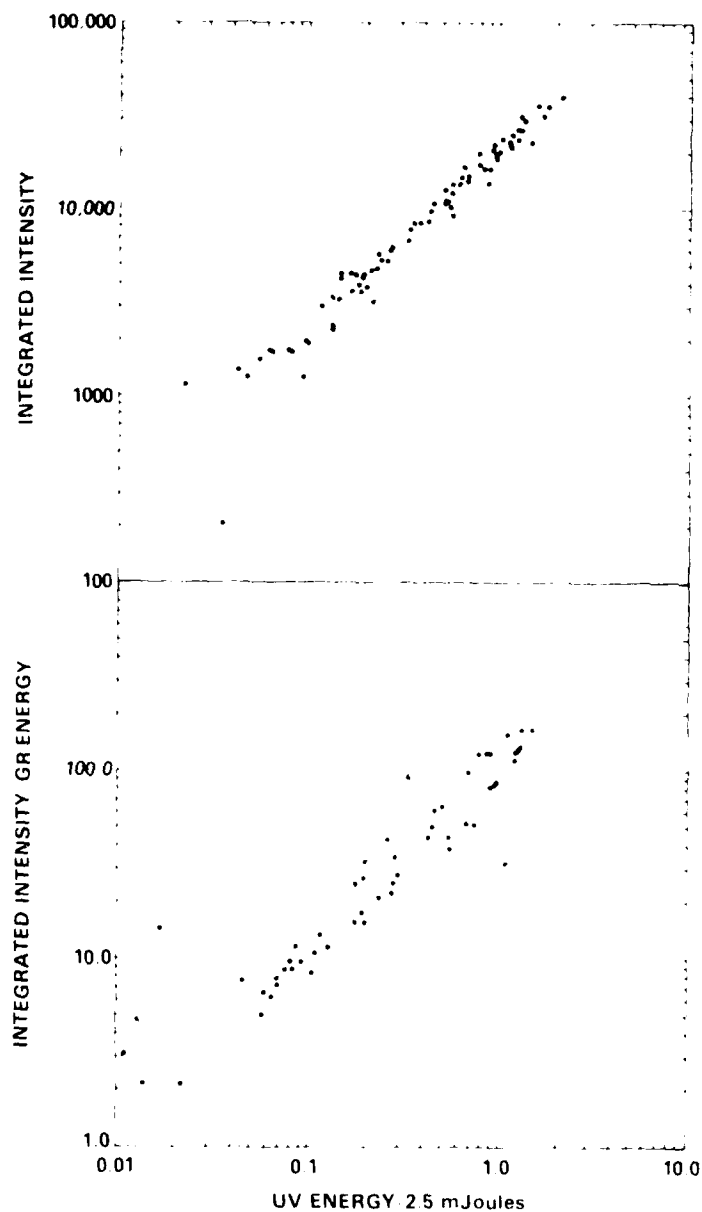
Fig. 3 - Solid line: LIF signal as a function of probe time delay for nitro-
methane at 0.8 Torr. Intensity is normalized to UV and probe pulse energies.
Each data point represents an average of 10 laser shots. Dashed line: system
temporal response function (see text) determined by photobleaching experiment
in rhodamine dye solution.

sents the time-integrated fluorescence intensity averaged over ten laser shots and normalized to the UV and probe pulse energies. The non-zero fluorescence signal for negative delay times represents the effect of the UV pulse alone.

We have estimated the quantum yield for formation of NO_2 in our experiment to be on the order of 1%. This is the equivalent of 1 μTorr of NO_2 produced in the laser beam. The calculation assumes unity quantum efficiency for fluorescent re-emission of absorbed 527 nm quanta by unquenched NO_2. Only about 1% of the excited NO_2 molecules radiate before they are collisionally quenched at these pressures of nitromethane.

Discussion

In most early photolysis experiments on nitromethane the final products were determined by chemical analysis, in which case a large number of secondary products were found, including CH_3ONO, CH_2O, CH_3NO, NO, and N_2O [4,6,12]. This, and the dependence of the relative quantum yield of methyl nitrate [2] upon the exciting UV wavelength led to the suggestion that there are other primary photolysis processes besides (I), specifically: [6]

$$CH_3NO_2 \xrightarrow{h\nu} CH_2 = N \genfrac{}{}{0pt}{}{O}{OH} \rightarrow CH_2O + NOH \qquad (II)$$

and

$$CH_3NO_2 \xrightarrow{h\nu} CH_3NO + O \qquad (III)$$
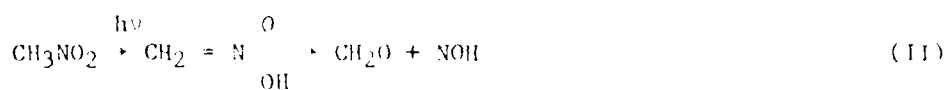
Rebbert and Slagg [2] suggested that more than one excited state of nitromethane was involved in its decomposition, and Honda et al. [6] and Flicker et al. [18] have supported this idea.

Three excited states of nitromethane have been experimentally identified and connected with its photolysis. Two are observed in the optical absorption spectrum [18-20]: a strong feature at 190 nm assigned to a π → π* transition, and a weak satellite at 260 nm suggested to be an n → π*, singlet-

57

singlet excitation. A third, still lower energy state has been found by
electron energy-loss spectroscopy [18] at ~ 326 nm, which the authors suggest
has $n \rightarrow \pi^*$, singlet-triplet character, but which may be a composite of
overlapping transitions of different character. Theoretical calculations
indicate that other transitions may exist in this energy region [21-24], but
they have not been identified experimentally.

Most investigators have supported process (I) as the main primary
photolysis channel for nitromethane [1-5]. Flicker et al. [18] and Honda et
al. [6] suggest that the lower energy transition to the triplet state at
~ 326 nm addresses process (I) particularly while the singlet-singlet
excitation near 260 nm induces reaction (II).

Both the experiment of Spears and Brugge [8] and our experiment used
photolyzing wavelengths in the vicinity of the 260 nm transition and both
observed the formation of some NO_2. However, considering the low quantum yield
estimated for NO_2 formation in our experiment, the possibility of other decay
channels cannot be excluded.

Summary

We have studied photolysis of nitromethane gas at pressures of < 3 Torr.
The photolyzing 264 nm pulse itself produces some NO_2 in an excited fluoresc-
ing state. Laser-induced-fluorescence probing using a time delayed second-
harmonic pulse reveals formation of a ground state NO_2 population in ~ 5 psec,
which remains roughly constant for probe delay times extending to 20 ns.
An estimate of quantum yield for the photodecomposition appears to be rather
low (~ 1%) at this photolyzing wavelength.

The observed fluorescence intensity scales linearly with UV pulse
energy. The LIF signal which monitors ground state NO_2 is also linear in both
UV and probe pulse energies.

Acknowledgments:

References

1. E. Hirschlaff and R. G. W. Norrish, J. Chem. Soc. 1580 (1936).

2. R. E. Rebbert and N. Slagg, Bull. Socs. Chim. Belges. 71, 709 (1962).

3. B. H. J. Bielski and R. B. Timmons, J. Phys. Chem. 68, 347 (1964).

4. I. M. Napier and R. G. W. Norrish, Proc. Roy. Soc. A299, 317, (1967).

5. R. B. Cundall, A. W. Locke and G. C. Street, in "The Chemistry of Ionization and Excitation," G. R. A. Johnson and G. Scholes, eds. (Taylor Francis, Ltd., London, 1967) p. 131.

6. K. Honda, H. Mikuni and M. Takahasi, Bull. Chem. Soc. Jpn. 45, 3534 (1972).

7. M. J. Collos, A. M. Annus, E. F. Marchaux, Nature, 229, 651 (1970).

8. K. G. Spears and S. P. Brugge, Chem. Phys. Lett. 54, 373 (1978).

9. N. S. Frist, L. S. Goldberg, T. R. Royt, L. N. Bradford, G. M. Shann, P. T. Stone and R. G. Weiss, in "Picosecond Phenomena," C. V. Shank, E. P. Ippen and S. L. Shapiro, eds. (Springer, N.Y. 1978) p. 23.

10. Ph. Avouris, A. Y. Chan and M. M. T. Loy, J. Photochem. 12, 177 (1980).

11. B. H. Rockney and E. R. Grant, Chem. Phys. Lett. 79, 15 (1981).

12. H. S. Kwok, G. Z. He, R. K. Sparks and Y. T. Lee, to be published in Int. J. Chem. Kinetics.

13. L. S. Goldberg, P. E. Schoen and M. J. Marrone, to be published.

14. G. E. Reverat, S. L. Leach and J. Cailhol, J. Chem. Phys. 56, 363 (1972).

15. V. M. Donnelly, D. G. Keil and F. Kaufman, J. Chem. Phys. 71, 659 (1979).

16. R. W. B. Pearse and A. G. Gaydon, "The Identification of Molecular Spectra," (Chapman and Hall, London, 1976).

17. R. Kandel, J. Chem. Phys. 23, 84 (1955).

18. W. M. Flicker, O. A. Mosher and A. Kuppermann, Chem. Phys. Lett. 60, 518 (1979).

19. S. D. Taylor, T. D. Allston, M. L. Moscato, G. B. Fazekas, R. Kozlowski, and G. A. Takacs, Int. J. of Chem. Kinetics, 12, 231 (1980).

20. S. Nagakura, Mol. Phys. 3, 152 (1960).

11.   J. W. Rabelais, J. Chem. Phys. 57, 960 (1972).

12.   L. E. Harris, J. Chem. Phys. 58, 5615 (1973).

13.   J. N. Murrell, B. Vidal and M. F. Guest, J. Chem. Soc. Faraday Trans.,
      II 71, 1577 (1975).

14.   K. L. McEwen, J. Chem. Phys. 32, 1801 (1961).

HIGH POWER PICOSECOND PHOTOLYSIS OF SIMPLE ORGANIC MOLECULAR GASES[*]

B.B. Craig[**], W.L. Faust, L.S. Goldberg, L.M. Schnur,
P.E. Schoen, and R.G. Weiss[**]

Naval Research Laboratory, Washington, DC 20375 U.S.A.
[**]Department of Chemistry, Georgetown University,
Washington, DC 20057 U.S.A.

ABSTRACT

High power picosecond ultraviolet pulses from a Nd:YAG
modelocked laser were used to induce a visible emission from a
variety of gaseous organic molecules. We report the observation
of electronically excited C_2, CH, CN, and H fragments. The
spectral characteristics and time development of the emitting
species are highly dependent upon the structure of the parent
molecules.

INTRODUCTION

Laser photolysis of simple molecules has contributed to a
deeper understanding of dynamical processes in photodissociation.
Our concern in the present work is with the decomposition of
simple compounds which afford generic models of processes
important in explosives, fuels, and other energetic materials.
Multiphoton IR and UV laser dissociation (1-4) have previously
been applied to study the primary decomposition processes of gas-
phase molecules and subsequent reaction of fragments having
significance in the kinetics of combustion. These experiments
have been performed in the nanosecond time domain and at millitorr
gas pressures in order to maintain a collision-free time regime

during the duration of the excitation pulse. In our experiments
the time resolution afforded by picosecond pulse excitation
enables such photolysis even at atmospheric pressures, yielding
high fragment concentrations. For the pressures and high flux
densities employed in this work, multiphoton absorption processes
can be accompanied by dielectric breakdown (5). Indeed, since
laser-induced breakdown is a nonresonant process, this very
nonspecificity facilitates the decomposition of a wide variety of
materials.

Here, we demonstrate the utility of the technique in
generating fragments whose emission spectra reflect their
precursors. We have carried out the photolysis of toluene,
methane, carbon monoxide, and nitromethane at pressures in the
range of 1-760 torr, and studied the luminescence from C_2, CH,
CN, and H fragments.

EXPERIMENTAL

Figure 1 shows a schematic of the Nd:YAG laser system. The
flashlamp-pumped oscillator, operating at a 1 Hz repetition rate,
employed a hybrid modelocking approach to provide more
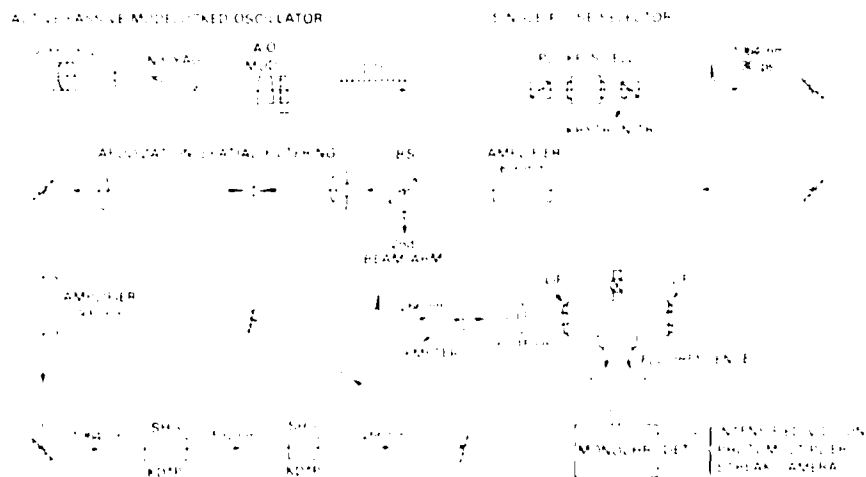reproducible pulse-train generation.

Figure 1. Schematic of the laser system.

It utilized an active acousto-optic loss modulator (Quantronix) and a passive saturable absorbing dye (Eastman A9740) in a flow cell. The single 1064 nm pulse, switched from near the peak of the train, had ca. 0.4 mJ energy and typically 30 ps duration. Two stages of amplification, apodization, and spatial filtering of the beam provided a high-spatial-quality IR pulse of 35-40 mJ energy. Efficient frequency doubling and redoubling in KD*P crystals generated a 4th harmonic (266 nm) photolysis pulse of up to 10 mJ energy. The laser beam was focused to a 0.15 cm diameter in a static gas cell (ca. 100 cm³) through a UV window. The emitted light generated from individual laser shots was collected at right angles and focused into a grating monochromator coupled to a Nuclear Data ND100 intensified silicon multi-channel recording system (spectral sensitivity 350-850 nm). Improved signal-to-noise was achieved where necessary by accumulating data from typically 30 laser shots. High-resolution spectra were obtained with a Spex 0.8 m monochromator (0.1 nm system resolution). For time-resolved studies, a Varian VPM-154M crossed-field photomultiplier was coupled to the exit slit of the monochromator. The transient signal was displayed on a Tektronix 7104 oscilloscope, giving a detection risetime of 400 ps. Observations were also made with an Electrophotonics streak camera (S-20 photocathode) having time resolution of 10 ps.

Methane was research grade purity supplied by Matheson Gas Products and was used without further purification. Carbon monoxide was ultra-high purity grade (Matheson) and was freed of any metal carbonyl contaminants by passing through a heated tube (200°C, atmospheric pressure) packed with glass wool (6). Nitromethane was Baker reagent grade and was distilled under nitrogen, collecting the middle fraction, b.p. 101-102°C. Ketene, CH_2CO was prepared by a standard procedure (7) involving dehydration of acetic anhydride at 500-550°C and was purified by trap-to-trap distillation. It was stored in the dark under vacuum in a liquid nitrogen bath. A salt-ice bath placed between the reservoir and the sample cell was used to condense traces of acetic acid and other high-boiling impurities.

RESULTS AND DISCUSSION

High power, 30 ps pulses at 266 nm focused into the vapors under study (10-500 torr) generated a visible streak near the focal region. Low- and high-resolution spectra of the luminescence exhibited no differences in intensity or spectral distribution during a typical experiment involving several hundred laser shots. This indicates that stable photolytic products do not significantly affect the primary decomposition processes. The result is not surprising since the photolyzed region is at least 10^6 smaller than the total sample volume. It should be emphasized that our analytical techniques give evidence only of luminescent species; other intermediates are undoubtedly produced.

Figure 2 depicts the similarity of the low-resolution emission spectra from ketene and carbon monoxide, each at 100 torr. High resolution spectra indicate that the predominant emission belongs to the C_2 diradical in its triplet $d^3\pi_g \to a^3\pi_u$ Swan transition (8).
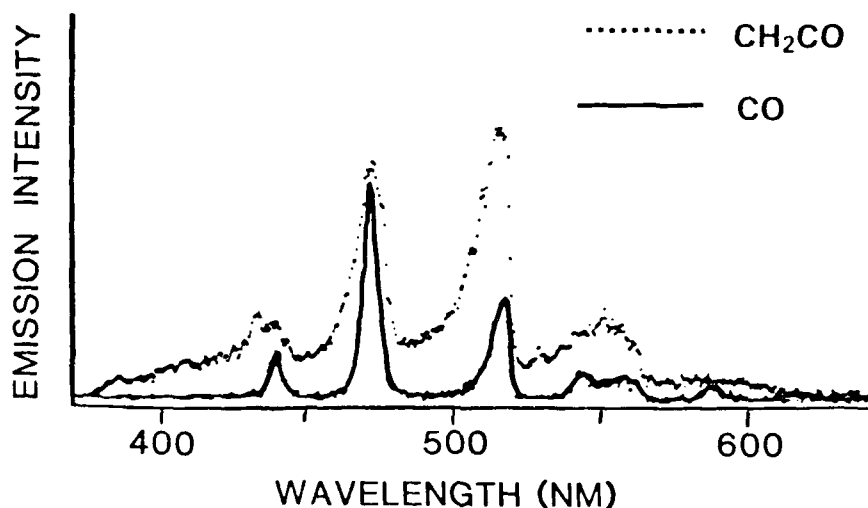
Figure 2. Low-resolution (2 nm) emission spectra obtained when ketene and carbon monoxide, at 100 torr, are irradiated with individual laser pulses at 266 nm.

Figures 3 and 4 show the $\Delta v = 0$ and $\Delta v = -1$ transitions for C_2 from carbon monoxide, methane, and ketene. The emission spectra from methane and ketene exhibit a strong attendant rotational structure. In addition, a weak, underlying continuum emission, associated with a plasma formation, extended throughout the visible region. The intensity of this background varied for each gas studied but was most prominent for methane. Figures 5 and 6 compare the regions of Swan $\Delta v = +1$ and $\Delta v = +2$ emission from carbon monoxide and ketene. Striking dissimilarities are evident at this resolution. Only in the case of CO are the C_2 "high-pressure" bands (9) observed. These are a consequence of the selective population of an upper vibrational level (generally attributed to $v' = 6$) (9) of the $d^3\pi_g$ state and necessitate distinct formation mechanisms for the C_2 produced from carbon monoxide and ketene.

55

C₂ SWAN SYSTEM
$d^3\pi_g - a^3\pi_u \quad \Delta\nu = 0$

CO

CH₄

CH₂CO

500.4   2,2   1,1   0,0   521.7

WAVELENGTH (NM)
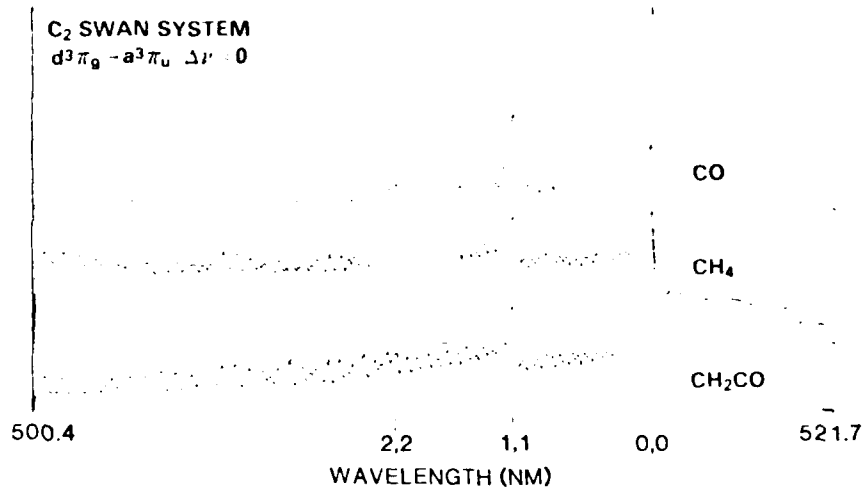
Figure 3.   High-resolution (0.1 nm) spectra of the Swan system emission ($\Delta\nu = 0$) derived from 266 nm irradiation of carbon monoxide, methane, and ketene, at 100 torr.   Data are accumulated from 30 laser shots.   Note the strong rotational decoration, to the high-energy side of the band heads, for methane and ketene.

C₂ SWAN SYSTEM
$d^3\pi_g - a^3\pi_u \quad \Delta\nu = -1$

CO

CH₄

CH₂CO

545.7   4,5   3,4   2,3   1,2   0,1   566.4

WAVELENGTH (NM)
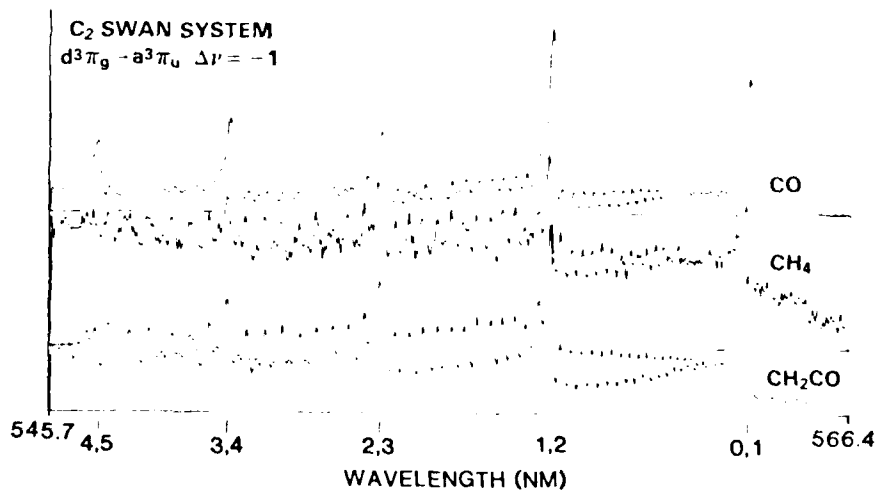
Figure 4.   Spectra of the Swan system emission ($\Delta\nu = -1$). Conditions as in Figure 3.
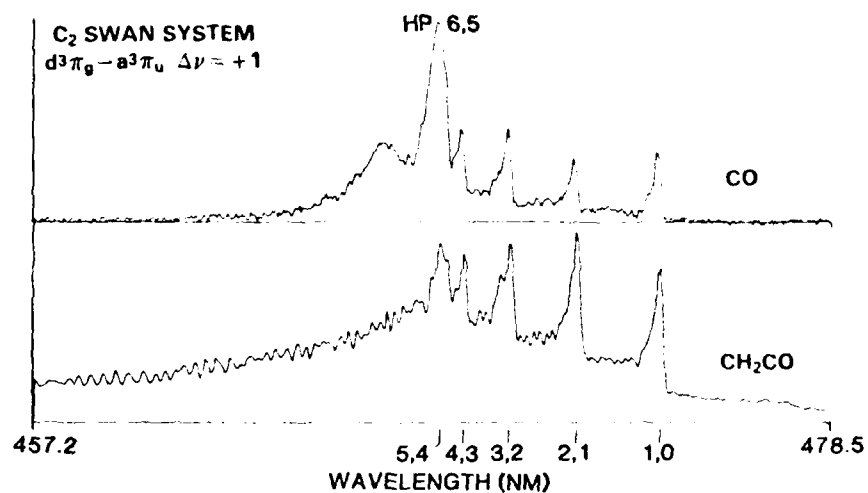
Figure 5. Spectra of the Swan system emission ($\Delta v = +1$) derived from carbon monoxide and ketene, at 100 torr. Data are accumulated from 30 laser shots. The spectrum from CO also shows the high-pressure 6,5 band.
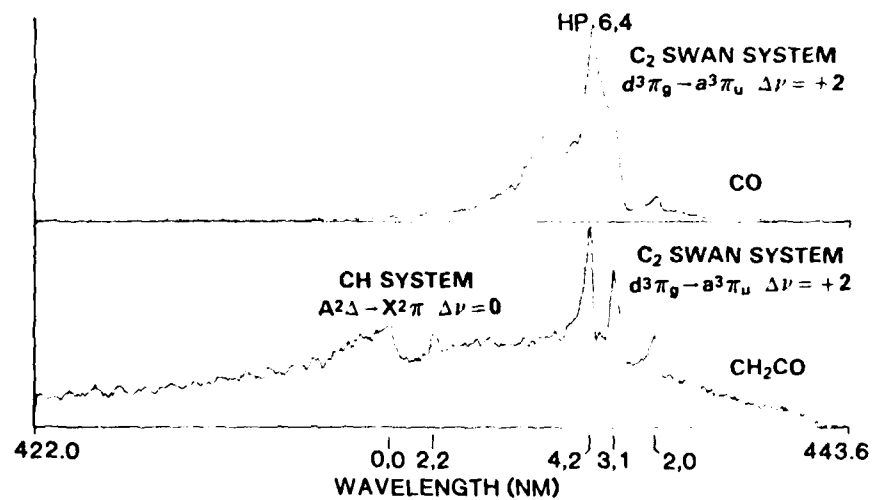
Figure 6. Spectra of the Swan system emission ($\Delta v = +2$). Conditions as in Figure 5. The spectra also show the high-pressure 6,4 band and CH emissions.

57

This difference of mechanisms finds further expression in the time-dependent oscilloscope data shown in Figure 7.
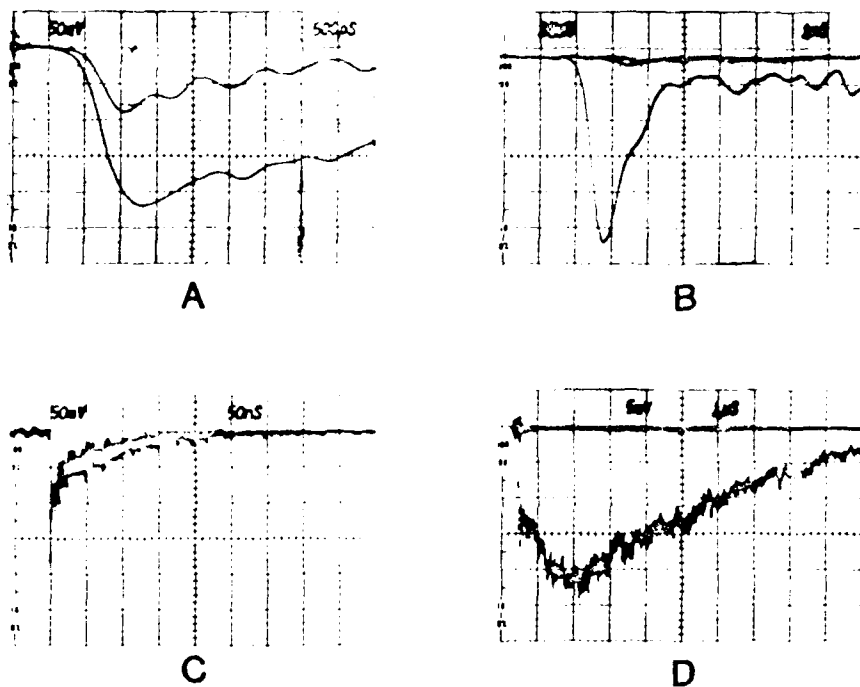
Figure 7. Oscilloscope traces of the C_2 Swan emission monitored at 516 nm (0,0 transition). A: ketene, 100 torr, 500 ps/div. The upper trace shows the plasma radiation at 516 nm. B: CO, 100 torr, 1 ns/div. C: ketene, 100 torr, 50 ns/div. D: CO, 100 torr, 1 µs/div.

Figure 7A shows the risetime-limited formation of the $d^3\Pi_g$ emissive state (at 516 nm) of C_2 derived from ketene. The risetime is indistinguishable from that of the plasma radiation

(upper trace), monitored at 616 nm where Swan emission is negligible. By contrast, no prompt C_2 emission is seen from CO (Fig. 7B) when either the normal or the high-pressure Swan bands are monitored. The oscillogram in Figure 7B shows only the brief plasma emission, which can be detected throughout the visible region. Over much lower timescales (Fig. 7D), the slow, collisional formation of the $d^3\pi_g$ state is observed. An intermolecular pathway leading to the formation of C_2, like that suggested by Kung et al. (10) (Eq. 1 and 2), is consistent with these data:

$$C + CO + M \rightarrow C_2O + M \tag{1}$$

$$C_2O + C \rightarrow C_2^* + CO \tag{2}$$

M represents a third body and * refers to an unspecified electronic state of C_2. The highly-specific vibrational population of the excited state is then rationalized as follows: there is a relaxation of the initial C_2 state to $b^3\Sigma_g^-$ which crosses $d^3\pi_g$ near its sixth vibrational level (11). It has generally been accepted that the high-pressure emission originates from $v' = 6$. However, the high-pressure bands lie to the low energy side of the corresponding normal Swan band head, where there are no rotational term differences. For example, the designated 6,5 high-pressure transition is at 468.0 nm while the regular 6,5 Swan band is observed at 466.9 nm (8,12). On this basis, we infer that the exact crossing between the $b^3\Sigma_g^-$ must occur below $v' = 6$.

Since the $d^3\pi_g$ state collision-free lifetime has been determined as ca. 120 ns (3), it is clear that the slower decay in Figure 7D does not reflect the kinetics of the $d^3\pi_g \rightarrow a^3\pi_u$ transition. Evidently we are following the formation and decay steps of an intermediate (consistent with Equation 1 and 2), which become the rate-determining processes for the C_2 $d^3\pi_g$ emission. Figure 7C indicates that the C_2 $d^3\pi_g$ state has a lifetime of ca. 70 ns when produced in 100 torr of ketene. It is likely that the parent molecule and/or other photolysis fragments are involved in quenching steps. For instance, all the hydrogen bearing gases exhibit a strong pressure-broadened emission line at 656.3 nm, assigned to the Balmer Hα line of atomic hydrogen (Fig. 8).

Returning to Figure 7A, the C_2 derived from ketene appears with detection-system risetime (the contribution of the plasma to the lower trace is limited). Such prompt C_2 formation suggests a unimolecular mechanism. However, a rapid collisional formation may be envisaged if the reacting fragments are created with substantial kinetic energy. Attempts to observe the formation using a streak camera have proved inconclusive. The spectral resolution required to minimize the prompt background has not allowed sufficient signal to be detected from the C_2 emission. In

the case of methane, where C_2 production must be a collisional process, we have nonetheless been unable to follow it kinetically. The plasma radiation dominates the transient signal at 100 torr of methane for several nanoseconds, by which time the C_2 signal is fully developed.
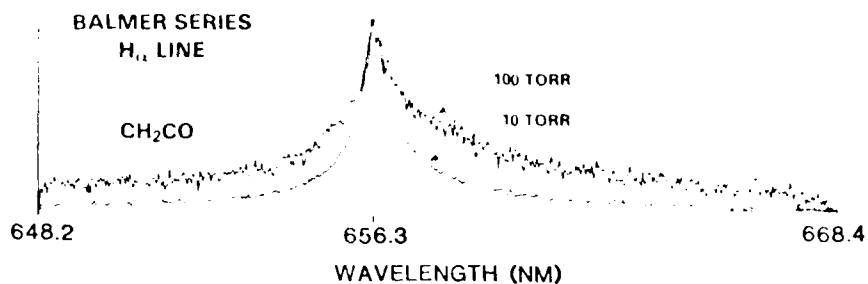
BALMER SERIES
H_α LINE

CH₂CO

100 TORR

10 TORR

648.2   656.3   668.4

WAVELENGTH (NM)

Figure 8. Spectra of the atomic hydrogen Hα emission line derived from 266 nm irradiation of ketene. Note the strong pressure-broadening effect.

The C_2 emission from methane and ketene show considerable rotational excitiation, which implies a non-thermally-equilibrated population of excited C_2 molecules. C_2 emission spectra showing such abnormal rotation are ubiquitous in discharge (13) and laser photolysis (3) studies of simple organic molecules. In an intermolecular mechanism, "off-axis" collisions between fragments would be expected to impart excess rotation to a C_2 product. It is also possible that ketene undergoes unimolecular elimination of hydrogen and oxygen via out-of-plane bending motions, leaving C_2 with rotation. In the case of CO, the C_2 high-pressure system is obtained together with the normal Swan system, both showing the same protracted time development. This now gives temporal as well as spectral inference that C_2 is formed from CO by processes entirely distinct from those in ketene and methane. Consequently, it is not surprising that the emission spectrum exhibits much less rotational fine structure than that derived from ketene and methane.

Weak lines were observed at 410.2 nm and 406.8 nm only when ketene was photolysed. They are attributed to the Deslandres-d'Azambuja singlet C_2 system ($C^1\eta_g \rightarrow A^1\eta_u$, $\Delta v = -1$) (8). A weak fluorescence at 431.4 nm (Fig. 6), observed for ketene and methane is attributed to CH emission ($A^2\Delta \rightarrow X^2\eta$, $\Delta v = 0$) (8).

The power dependence of the C_2 emission is displayed in Figure 9. At high input pulse energies, both carbon monoxide and ketene (100 torr) show a near-linear power dependence indicative

of a saturation regime. The high-order nature of the excitation process is clearly evident from the steepening of the curves towards lower input energies. Furthermore, focusing of the excitation beam was essential for producing observable emission. Carbon monoxide and methane showed no emission at pressures below 10 torr. Ketene, however, which possesses a single-photon transition at 266 nm ($\epsilon \sim 0.5$ mol^{-1} cm^{-1}) (14), exhibited luminescence even at pressures below 1 torr. The streak of visible emission extended somewhat beyond the focal region and had a more diffuse appearance than that observed at higher pressures. The excitation processes may well be different at lower pressures, but the observed luminescent products appear the same.
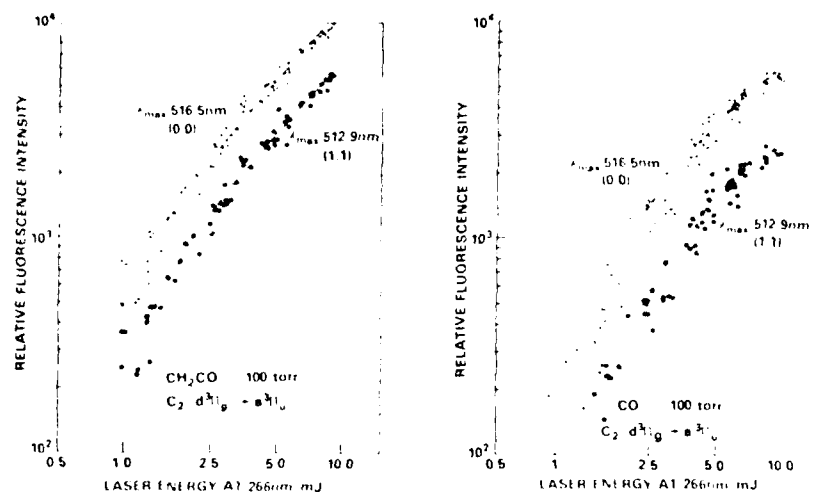

Figure 9. Dependence of the C_2 Swan emission intensity on input laser pulse energy at 266 nm, from ketene (left) and carbon monoxide (right), at 100 torr.

Figure 10 compares the $\Delta v = 0$ C_2 Swan system observed from 15 torr of nitromethane with that from 10 torr of ketene. The C_2 band is substantially weaker in the case of nitromethane. It shows excess rotational excitation, as for ketene and methane. Furthermore, two new strong emissions were observed with band heads at 421.6 nm and 388.3 nm (Fig. 10, below). These are assigned to the violet system of CN and arise from $B^2\Sigma^+ \rightarrow X^2\Sigma^+$ transitions (8). The $\Delta v = 0$ transition was also weakly observed in the case of ketene and carbon monoxide, indicating a slight nitrogen impurity.
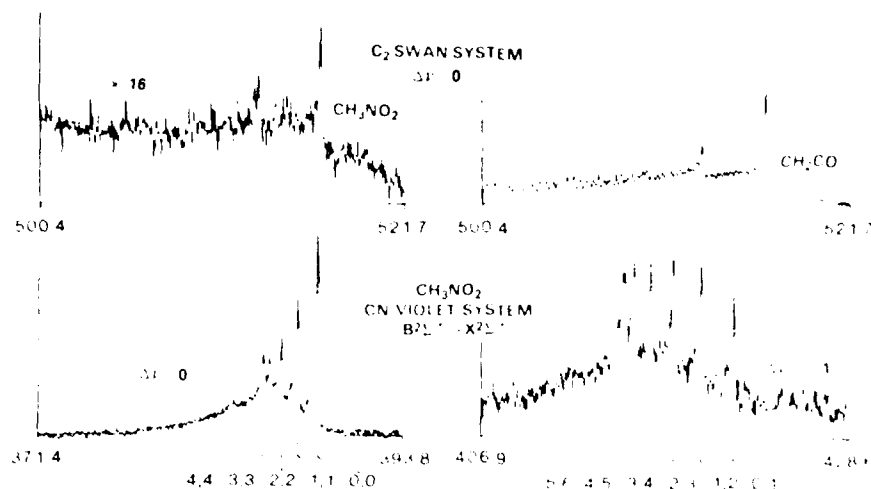
Figure 10. Above: Spectra of the C_2 Swan emission ($\Delta\nu = 0$) derived from ketene at 10 torr and nitroethane at 15 torr. Note the reduced intensity of the signal from nitroethane. Below: Spectra of the CN violet system emission ($B^2\Sigma^+ - X^2\Sigma^+$, $\Delta\nu = 0, -1$) derived from nitroethane at 15 torr. Data are accumulated from 30 laser shots.

The appearance of the strong CN emission from nitroethane and corresponding decrease in the C_2 emission might indicate that even under these harsh excitation conditions, the C-N bond remains intact. On the other hand, observations from conventional photolysis have been interpreted to support scission of the C-N bond as the main primary process (15). The CN fragment from nitroethane could be generated unimolecularly, whereas by necessity C_2 is produced collisionally. Experiments are now in progress to follow the time development of the CN emission. In addition, we are examining other nitro-bearing alkanes which could provide an intramolecular C_2 formation pathway as a competing process with CN production.

SUMMARY

In this work we have extended to the picosecond regime the time definition for laser initiation and interrogation of gas-phase molecular dissociation, with spectral resolution adequate to isolate individual fragment species and indeed to observe

rotational structure. We have examined the spectral and temporal characteristics of the dominant emitting fragments, C_2, CH, CN, and H_2 observed in intense picosecond UV irradiation of ketene, methane, carbon monoxide, and nitromethane. The rapid production of the C_2 $d^3\Pi_g$ state from methane and ketene (limited by the detection system risetime) suggests a similar mechanism of collisional formation, although a unimolecular process can not be ruled out in the case of ketene. Photolysis of CO also yields the C_2 $d^3\Pi_g$ state, which develops and decays collisionally over several microseconds. Its spectrum exhibits the Mulliken pressure bands and shows much less rotational excitation than that obtained from ketene and methane. It is possible that a rotationally nonthermalized C_2 $d^3\Pi_g$ population can be constructed from precursors bearing CH_x. For this reason, future studies of the weak C_2 signal and its temporal characteristics should give some insight into the possible free radical pathways. Future application of this technique to these simple diatomic and other related compounds may provide important information on reactions through which these molecules participate in the early phases of rapid decomposition.

REFERENCES

1. Ambartzumian, R.V., Chekalin, S.V., Letokhov, V.S., and Ryabov, E.A.: 1975, Chem. Phys. Lett. 36, pp. ...

2. Lesiecki, M.L., and Guillory, W.A.: 1977, J. Chem. Phys. 66, pp. 4317-4322.

3. McDonald, J.R., Baronavski, A.P., and Donnelly, V.M.: 1978, Chem. Phys. 33, pp. 161-170.

4. Filseth, S.V., Hancock, G., Fournier, J., and Meier, K.: 1979, Chem. Phys. Lett. 61, pp. 288-292.

5. Ronn, A.M.: 1976, Chem. Phys. Lett. 42, pp. ...

6. Braker, W., and Mossmann, A.L.: 1971, "Matheson Gas Data Book."

7. Nutall, R.L., Laufer, A.H., and Kilday, M.V.: 1971, J. Chem. Thermodyn. 4, pp. 167-174.

8. Pearse, R.W.B., and Gaydon, A.G.: 1965, "Identification of Molecular Spectra," Chapman and Hall, London.

9. Herzberg, G.: 1946, Phys. Rev. 70, pp. 762-764.

10. Kunz, C., Harteck, P., and Dondes, S.: 1967, J. Chem. Phys. 46, pp. 4157-4158.

11. Read, S.M., and Vanderslice, J.T.: 1962, J. Chem. Phys. 36, pp. 2366-2369.

12. Johnson, R.C.: 1927, Phil. Trans. Royal Soc. A 266, pp. 157-230.

13. Lochte-Holtgreven, W.: 1930, Z. für Physik. 64, pp. 443-451.

14. Laufer, A.H., and Keller, R.A.: 1971, J. Am. Chem. Soc. 93, pp. 61-63.

15. Honda, K., Mikuni, H., and Takahasi, M.: 1972, Bull. Chem. Soc. Japan, 45, pp. 3534-3541.

DATE FILMED

4-8